الجمهورية الجزائرية الديمقراطية الشعبية
PEOPLE'S DEMOCRATIC REPUBLIC OF ALGERIA
وزارة التعليم العالي والبحث العلمي
Ministry of Higher Education and Scientific Research
جامعة ابي بكر بلقايد –تلمسان-
University of Abou Bekr Belkaid – Tlemcen –
Faculty of Technology

THESIS

Presented for obtaining the **Master's** degree
In : Mechanical engineering

Specialty : Energetics
By : EL HABIRI Amel.

Subject

Numerical Simulation of a Compact Indirect Solar Dryer

Publicly defended on 25/06/2025, in front of the jury composed of:

Mr. GUELLIL Hocine	MCA	Univ. Tlemcen	President
Mme. SARI HASSOUN Hind	MAA	Univ. Tlemcen	Supervisor
Mr. KORTI Abdel Illah Nabil	Pr.	Univ. Tlemcen	Co-supervisor
Mr. BEGAG Abdelaziz	MCB	Univ. Tlemcen	Examiner

Academic year:2024 /2025.

DEDICATION

I dedicate this thesis, with all my love and gratitude : To
my dear mother,
a source of love, patience, and prayers,
you who have always believed in me, even when I doubted myself, you
whose silent sacrifices allowed me to move forward...
I dedicate this work to you with all my heart.
May God protect you, shower you with His mercy, and reward you for all that you are and all that you do.

To my dear father,
a model of wisdom, perseverance, and generosity, you who
have always supported me without ever wavering, you
whose often quiet efforts paved the way for me...
I dedicate this work to you with deep gratitude and immense respect.
May God reward you for your love, patience, and sacrifices.

To my sister Safaa, for her reassuring presence, her encouragement, and her tenderness, which often comforted me during difficult moments.
To my brother Hichem, for his support, kind words, and constant care.

And to all those who supported me, directly or indirectly, throughout this academic journey.
Your words, your actions, and your trust have been invaluable sources of
motivation

ACKNOWLEDGMENT

First and foremost, I thank Allah, the Creator of all things, for granting me the health, patience, and perseverance needed to complete this thesis.

I would like to express my deepest gratitude to my supervisor, Mme. SARI HASSOUN Hind, for her availability, valuable advice, rigorous guidance, and constant support throughout this work.

My sincere thanks also go to my co-supervisor, Professor KORTI Abdel Ilah Nabil, for his insightful guidance, close supervision, and invaluable assistance in carrying out this project.

Special recognition goes to the committee members, Mr. GUELLIL Hocine and Mr. BEGAG Abdelaziz, for their thorough evaluation and kind presence at our presentation.

I warmly thank Mr. BENRAMDANE Mohammed, Head of the Mechanical Engineering Department, for the resources made available to us and for the quality of the educational environment provided.

I do not forget all the faculty members and staff of the department for the quality of their teaching, their support, and their kindness throughout my university journey.

I would like to express my heartfelt gratitude to my parents for their unconditional love, sacrifices, patience, and moral support throughout my life.

A loving thought goes to my sister and brother, who have always encouraged and supported me, even during difficult times.

I would also like to extend my profound thanks to my dear friends ZERRADI Rania and CHEBOUROU Nour El Houda for their unwavering support throughout this journey. Their sincere friendship has been a source of inspiration and constant motivation. Thank you for your kindness, your positive spirit, and for believing in me.

To all of you — thank you.

الملخص

تتناول هذه الدراسة تحليل السلوك الحراري الديناميكي لمجفف شمسي غير مباشر مدمج .
وتهدف إلى وصف ظواهر انتقال الحرارة داخل النظام، مع التركيز بشكل خاص على آليات التوصيل الحراري المضطر والطبيعي، بالإضافة إلى توزيع درجات الحرارة داخل مكونات المجفف المختلفة. يعتمد الجهاز المدروس على مجمّع شمسي حراري متصل بغرفة تجفيف معزولة، مما يسمح بانتقال الحرارة من خلال تدفق هواء ساخن، دون تعريض المنتج مباشرةً للإشعاع الشمسي. تتم دراسة المحاكاة العددية المدعومة ببيانات تجريبية، من أجل تقييم الكفاءة الطاقوية للنظام وتحسين معاملات التشغيل .

الكلمات المفتاحية: مجفف شمسي غير مباشر مدمج، السلوك الحراري الديناميكي، محاكاة عددية

Abstract

This study focuses on the analysis of the thermo-dynamic behavior of a compact indirect solar dryer. The objective is to characterize the heat transfer phenomena occurring within the system, with particular emphasis on the mechanisms of forced and natural convection, as well as the temperature distribution within the different components of the dryer. The studied device is based on a thermal solar collector coupled with an insulated drying chamber, allowing heat transfer through a flow of heated air without direct exposure of the product to solar radiation. A numerical simulation approach, possibly supported by experimental data, is considered in order to evaluate the energy efficiency of the system and optimize its operating parameters.

Keywords: compact indirect solar dryer, dynamic thermal behavior, forced and natural convection, numerical modeling.

Résumé

Cette étude porte sur l'analyse du comportement thermo-dynamique d'un séchoir solaire indirect compact. L'objectif est de caractériser les phénomènes de transfert de chaleur intervenant dans le système, en mettant particulièrement l'accent sur les mécanismes de convection forcée et naturelle, ainsi que sur la distribution des températures au sein des différentes composants du séchoir. Le dispositif étudié repose sur un capteur solaire thermique couplé à une chambre de séchage isolée, permettant un transfert de chaleur par l'intermédiaire d'un flux d'air chauffé, sans exposition directe du produit au rayonnement solaire. Une simulation numérique, éventuellement couplée à des données expérimentales, est envisagée afin d'évaluer l'efficacité énergétique du système et d'optimiser les paramètres de fonctionnement.

Mots clés : séchoir solaire indirect compact, comportement thermique dynamique, convection forcée et naturelle, Modélisation numérique

Table of Contents

General introduction 1

Chapter I: Drying Technologies – Principles and Literature Review

I.1. Introduction 4
I.2. Definition of drying 4
I.3. Drying rate 4
I.4. Drying Mechanism 6
I.5. Different Drying Methods..... 6
I.5.1. Convection Drying 7
I.5.2. Conduction Drying 7
I.5.3. Radiation Drying 8
I.6. Fields of Application of Drying 8
I.6.1. Agri-food Indust 8
I.6.2. Wood Industry 9
I.6.3 Food and Pharmaceutical Industries 9
I.7. Type of Drying 10
I.7.1. Direct solar drying 10
I.7.2.Indirect Solar Drying 11
I.8. Solar Dryer 11
I.8.1. Definition 11
I.8.2. Different Types of Solar Dryers 11
I.8.2.1. Direct Solar Dryer 12
I.8.2.2 Indirect Solar Dryer 13
I.8.2.3 Passive Solar Dryers (Natural Convection) 15
I.8.2.4. Active Solar Dryer (or Forced Convection Dryer) 15
I.8.2.5 Mixed solar dryer..... 16
I.9. Literature Review 16
I.10. Conclusion 29

Chapter II: Physical Model, Mathematical Formulation, and Numerical Resolution

II.1. Introduction 31
II.2. Physical Model 32
II.3. Simplifying Assumptions 34
II.4. Mathematical Model 34

II.4.1. In the Air 34
II.4.2. Energy conservation equation in the absorber and glazing..... 35
II.5. Initial and boundary conditions 36
II.5.1.Equation of ambient temperature variation as a function of time: 36
II.5.2. Equation of global solar radiation variation as a function of time 36
II.5.3. Initial Condition 38
II.5.4. Boundary Conditions 38
II.6. Simulation using FLUENT 39
II.6.1. Geometry 39
II.6.2 Choice of solver type : 39
II.6.3 Choice of material : 40
II.6.4. Solver Controls: 41
II.6.5. Pressure-Velocity Coupling : 42
II.7. Mesh test 42
II.8. Conclusion 44

Chapter III: Numerical Results, Analysis, and Interpretation

III.1. Introduction 46
III.2. Validation of Numerical Results 46
III.3. Effect of Air Velocity and thermal Behavior 48
- of 0.55 m/s : 48
- of 0.65 m/s : 50
- of 0.45 m/s : 51
- of 0.1 m/s: 53

III.4. Dynamic Behavior : 55
III.5. Effect of the Fan Position : 56
III.5.1. Velocity behavior 57
III.5.2. Thermal and Dynamic Behavior: 58
III.6. Collector Efficiency 59
III.7. Drying Chamber Efficiency……..61
III.8.conclusion…… .62
General conclusion 63
References 66

List of Figures

Figure I.1: Drying rate curves for phases I, II, and III. 5
Figure I.2: Wood drying. 9
Figure I.3: Drying of food and pharmaceutical products. 9
Figure I.4: Direct solar drying of seedless black Corinthian grapes on a concrete threshing floor in open air. 11
Figure I.5: Direct solar dryer. 12
Figure I.6: Principle of a direct solar dryer. 13
Figure I.7: Indirect solar dryer. 14
Figure I.8: Schematic diagram of an indirect solar dryer. 14
Figure I.9: Examples of direct and indirect solar dryers using natural convection and forced convection modes. 16
Figure I.10: Direct solar dryer with a chimney. 17
Figure I.11: Functional architecture of a direct-mode solar dryer with a chimney. 18
Figure I.12: Diagram of a solar dryer. 19
Figure I.13: Representation of the auxiliary energy system installation. 19
Figure I.15: Temperature distribution in the direct solar dryer without PCM. 21
Figure 16: Temperature distribution in the direct solar dryer with PCM..... 21
Figure I.17: (a) Experimental solar dryer, (b) Drying tray, (c) Thermal resistance analogy of the solar collector envelope. 22
Figure I.18: (a) Photos of the tested solar dryer, (b) Final dried product from each trial. 23
Figure I.19: Prototype of the constructed solar dryer. 24
Figure I.20: Schematic diagram of the dryer with PCM integration in the collector. 25
Figure I.21: Temperature field inside the dryer with and without PCM in the collector. 25
Figure I.22: Schematic diagram of the dryer with PCM integration in the solar chimney. 26
Figure I.23: Temperature field inside the dryer with and without PCM in the solar chimney. 26
Figure I.24: Schematic diagram of the solar dryer integrating a thermal bed. 27
Figure I.25: Temperature contours and streamlines inside the solar dryer with thermal bed. 28
Figure I.26: Temperature contours and streamlines inside the solar dryer with two air inlets. 28
Figure I.27: Mixed-mode solar dryer.. 29

Figure II.1: Prototype of the constructed solar dryer 31
Figure II.2: Schematic diagram of the solar dryer 32
Figure II.3: Diagram of the physical model of an indirect solar dryer 33
Figure II.4: Temporal evolution of ambient air temperature 36
Figure II. 5: Temporal evolution of solar radiation 37
Figure II.6: Geometry of the Solar Dryer Modeled in ANSYS Fluent 19..... 39
Figure II.7: General solver configuration in ANSYS Fluent 39
Figure II.8: Definition of the thermophysical properties of air in ANSYS Fluent 40
Figure II.9: Definition of the thermophysical properties of steel in ANSYS Fluent 40
Figure II.10: Definition of the thermophysical properties of glazing in ANSYS Fluent 41
Figure II.11: Transient calculation control parameters 41
Figure II.12: Selection of the pressure-velocity coupling scheme in ANSYS Fluent 42

Figure II.13: Comparison of Absorber Temperature Over Time for Different Time Steps (dt = 5s, 10s, 15s) with Experimental Data 42
Figure II.14: Comparison of absorber temperatures for different mesh configurations and experimental data 43

Figure III.1: Comparison of Numerical and Experimental Temperature Results 46
Figure III.2: Behavior of the air velocity field in our solar dryer 48
Figure III.3: Distribution of temperature and velocity vectors in the dryer 49
Figure III.4: Behavior of the air velocity field in our solar dryer 50
Figure III.5: Distribution of temperature and velocity vectors in the dryer 51
Figure III.6: Behavior of the air velocity field in our solar dryer 51
Figure III.7: Distribution of temperature and velocity vectors in the dryer 52
Figure III.8: Behavior of the air velocity field in our solar dryer 53
Figure III.9: Distribution of temperature and velocity vectors in the dryer 54
Figure III.10: a) Absorber Temperature Distribution for Different Inlet Velocities (0.65, 0.55, 0.45, and 0.1 m/s) .b) Drying Chamber Temperature Distribution for Different Inlet Velocities (0.65, 0.55, 0.45, and 0.1 m/s) 55
Figure III.11: Behavior of the air velocity field in our solar dryer 57
Figure III.12: Distribution of temperature and velocity vectors in the dryer with fan 58
Figure III.13: Evolution of the thermal efficiency of the solar collector throughout the day 60
Figure III.14: Evolution of the thermal efficiency of the drying chamber throughout the day 61

List of Tables

Table II. 1: Dimensions of the glazing and absorber of the solar dryer 33
Table II. 2: Thermophysical Properties of the Solar Dryer 33
Table II. 3: Characteristics of the Meshes Used 43

Table III. 1: Mean Relative Errors of Simulated Temperatures 47

Nomenclature

Latin Letters		Unit
A_c	Collector surface	[m^2]
C_p	Specific heat	[J / Kg.K]
e	Thickness	[m]
G	Solar radiation	[W/m^2]
h_c	Convective heat transfer coefficient	[$W/m^2.K$]
I	Incident solar radiation	[W/m^2]
g	Gravitational acceleration	[m / s^2]
$\dot{m}$	Mass flow rate of air	[Kg/s]
P	Pressure	[Pa]
Q	Heat quantity	[W]
Q	Radiative flux	[W/m^3]
S	Surface	[m]
t	Time	[s]
T	Temperature	[K]
T_a	Air temperature	[K]
T_a	Ambient temperature	[K]
T_s	Temperature of the product to be dried	[K]
u	x-direction velocity	[m/s]
v	y-direction velocity	[m/s]
x	Horizontal coordinate	[m]
y	Vertical coordinate	[m]

Greek Symbol

ρ	Density	[Kg / m^3]

λ	Thermal conductivity	[W / m.K]
μ	Dynamic viscosity	[Kg / m.s]
α	Absorption coefficient	
τ	Transmissivity coefficient	
ε	Emissivity	
β	Thermal expansion coefficient	
η_{co}	Thermal efficiency of the solar collector.	
η_{ch}	thermal efficiency of the drying chamber.	

Index :

g	glass
a	absorber

General Introduction

General introduction

Solar energy represents a renewable, clean, and inexhaustible energy source, widely available in most regions of the world. Harnessed for centuries, it now stands as a promising alternative to fossil fuels, both for electricity generation and thermal applications, particularly in the agricultural sector.

Among these applications, solar drying stands out as an efficient and eco-friendly method for preserving agricultural products, particularly fruits, vegetables, and aromatic plants. This process involves removing the moisture contained in the products using solar energy, while preserving their nutritional and organoleptic qualities. It also helps reduce post-harvest losses, a crucial issue for rural areas and developing countries.

Solar dryers developed in this context come in various configurations depending on the method of heat collection and transfer. The indirect solar dryer is characterized by the fact that the air is heated in a solar collector before being directed to the drying chamber, without the products being directly exposed to solar radiation. This configuration allows for better control of the drying conditions, particularly temperature and airflow, and reduces the risk of product degradation.

Today, thanks to advances in numerical simulation, it is possible to accurately model the thermodynamic behavior of such systems before their experimental implementation. Computational Fluid Dynamics (CFD) provides powerful tools to analyze airflow, heat transfer, and to optimize dryer design. In this work, we used the ANSYS Fluent 19 software, known for its ability to solve the Navier-Stokes equations coupled with energy equations in complex geometries.

This study focuses on the analysis of the dynamic and thermal behavior of a compact indirect solar dryer. A numerical modeling approach, possibly coupled with experimental data, is considered in order to understand how heat is transferred within the system, as well as the evolution of temperatures and airflow over time, with the aim of optimizing the energy efficiency and performance of the dryer. This work is structured into three main chapter

- The first chapter presents general information on drying, the different types of solar dryers, and a literature review of previous research.
- The second chapter is devoted to the physical modeling, the mathematical formulation of the governing equations, and the numerical resolution of the problem using ANSYS Fluent 19.
- The third chapter presents a validation of the simulation results using experimental data, accompanied by detailed analyses and interpretations.

Finally, a general conclusion summarizes the main findings and offers some perspectives for improvement or further research.

Chapter I

Drying Technologies – Principles And Literature

I.1. Introduction

Drying is one of the most energy-consuming processes in the drying of agricultural and industrial products, where fuel or another conventional energy source is used to heat the air before drying the product. However, solar energy is a promising renewable energy source for drying, aiming to reduce energy consumption and carbon footprint during the drying process. It is also natural, abundant, sustainable, environmentally friendly, and cheaper than conventional drying methods. In tropical and subtropical regions, agricultural and marine food products such as fruits, vegetables, rice, nuts, fish, coffee, seeds, meat, etc., need to be dried in order to be preserved longer without compromising product quality. Thus, solar drying is widely used (e.g., from drying vegetables and fruits to wood and textile production, and from polymers and ceramics to pharmaceutical and mineral processing) and highly acceptable for performing such tasks. **[1]**

This chapter first presents the general principles of drying, then focuses on the operation and advantages of solar dryers. A literature review of the main research and technologies developed in this field is also provided in order to better understand the state of the art and recent developments.

I.2. Definition of drying

Drying a product consists of extracting a large portion of the water it contains until it reaches a sufficiently dry state that ensures proper preservation. Drying therefore helps to reduce or even eliminate post-harvest losses due to degradation. However, this process is often accompanied by changes in taste, appearance, and a loss of nutritional or hygienic quality of the product. **[2]**

I.3. Drying rate

The drying rate is a key parameter, influenced by both the temperature and moisture content of the product, as well as by the drying air conditions, particularly its temperature, relative humidity, and velocity. Since agricultural products are hygroscopic, controlling the drying rate is of particular importance.

The drying of a material generally follows two main phases.

- ✓ The first phase, known as the constant-rate phase, corresponds to an initial period during which the surface of the product remains saturated with moisture, allowing continuous evaporation as long as water is present on the surface.

- ✓ The second phase is the falling-rate phase, which begins as soon as the surface is no longer saturated, marking the critical point. At this stage, evaporation is limited by the migration of moisture from within the material to the surface.

- ✓ For hygroscopic products, a third phase is identified , corresponding to the second part of the falling-rate period. In this stage, the moisture content gradually decreases until it reaches an equilibrium state, at which point drying stops.

For most products, drying ends before reaching Phase III. The drying time for each period depends on the nature of the product and the drying conditions. Many food products do not exhibit a constant-rate phase at all, as many crops have an initial moisture content close to the critical point and quickly reach the critical point C (Fig. 1), where Phase II begins.

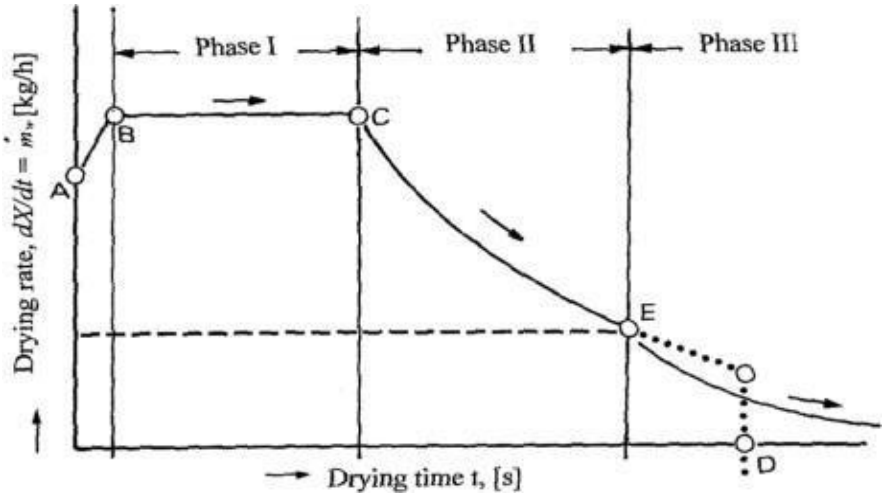

Figure I.1: *Drying rate curves for phases I, II, and III.*

Figure I.1 provides an overview of the three typical phases of a drying curve. Segment AB represents the time required to heat the material until it reaches the drying temperature. Segment BC corresponds to the constant-rate drying phase, while segment CE represents the falling-rate phase, during which the moisture flux from within the material gradually decreases. Point C is called the critical point: from this moment on, the surface of the product is no longer saturated with moisture, and the falling-rate phase begins.

At point E, moisture still remains inside the product; moisture transfer then occurs slowly through diffusion, and drying can stop—at point D, for example—once the desired final

moisture content is reached. For hygroscopic materials, the curve becomes asymptotic, and drying stops when hygroscopic equilibrium is achieved.

The duration of these different phases, for hygroscopic products, depends on the initial moisture content and the final moisture content required for safe storage. **[3]**

I.4. Drying Mechanism

The objective of drying, whether traditional or modern, is to significantly reduce the various reactions that contribute to the natural decomposition of the product. It is therefore necessary to remove a substantial portion of the water contained in the product. This water is expelled through evaporation into the surrounding atmosphere. This process requires thermal energy (solar, electric, or gas). The energy enables the water to move through the product, transform into water vapor, and be expelled to the outside in a closed dryer system.
Mastering the drying process therefore involves controlling several factors:

- The thermal energy (not too much, not too little) that causes the evaporation of water.
- The capacity of the surrounding air to absorb the water vapor released by the product (hence the difficulty of achieving proper drying during the humid season, as the air is already saturated).
- The ideal air velocity at the level of the product, in order to accelerate the removal of water vapor: drying must be done quickly to prevent product spoilage, but not too quickly to avoid the formation of à crust.
- The characteristics of the fresh product: oily fish are not dried the same way as fruits or vegetables.
- The quality of the fresh product to be dried upstream (supply, sorting, pretreatment) and the dried product downstream (packaging, storage, distribution chain). **[4]**

I.5. Different Drying Methods

To facilitate the drying process, it is generally necessary to supply the energy required to transform the liquid to be removed into vapor. Several drying methods are identified:
convection drying, conduction drying and radiation drying. **[5]**

I.5.1. Convection Drying

Convective drying involves transferring heat to the product through a heated fluid (usually air), which provides both the thermal energy and the removal of moisture in the form of vapor. The efficiency of the process strongly depends on the temperature, relative humidity, and the velocity of the airflow. The greater the temperature gradient and airflow speed, the faster the heat and mass transfer, thereby improving the drying rate. This type of transfer follows the equation :

$$Q = h\ S\ (T_a - T_s) \qquad \text{I.1}$$

Where :

- Q: the amount of heat transferred per unit of time. [W**]**
- S: the exchange surface area. [m²]
- $(T_a - T_s)$: the difference between the drying air temperature and the surface temperature of the product to be dried. [K]
- h : the convective heat transfer coefficient. [W / m²- K]

I.5.2. Conduction Drying

In this type of drying, heat is transferred directly to the product through contact with a hot surface. The resulting vapors are removed either by suction or by means of a slight gas flow. This gas moves slowly, unlike convective drying which requires a higher flow rate. If the temperature difference between the hot surface and the product is low, the contact surface must be increased to ensure effective heat transfer and efficient drying of the product.

The heat flux (in W/m²) is given by the following relation :

$$\frac{Q}{S} = -\lambda \frac{dT}{dx} \qquad \text{I.2}$$

Where:

- λ : thermal conductivity of the product film or the gas through which the heat transfer occurs. [W / m.K]

- $\frac{dT}{dx}$: Temperature gradient between the hot wall and the product.

I.5.3. Radiation Drying

In this drying method, the energy required for moisture evaporation is transferred to the product in the form of thermal radiation, usually infrared. This technique is particularly effective for the rapid removal of water, especially when the product is not heat-sensitive. Radiation sources can include gas-fired emitters, electric emitters (infrared lamps), or even solar radiation. This process allows for direct and uniform heating of exposed surfaces, with a rapid temperature rise.

$$q=\varepsilon\cdot\sigma\cdot(T_s^4-T_{env}^4) \quad \text{I.3}$$

Where **:**

- q: radiative heat flux [W/m²]
- ε : emissivity of the surface
- σ : Stefan–Boltzmann constant ($\sigma=5.67\times10^{-8}W/m^2\cdot K^4$)
- T_s : surface temperature [K]
- T_{env} **:** temperature of the environment or of the surrounding surfaces [K]

I.6. Fields of Application of Drying

I.6.1. Agri-food Indust

A large portion of the food we consume has undergone a drying process, which is often essential for its preservation and long-term stability. In the agri-food industry, nearly 200 types of industrial dryers are used, each adapted to different products and processes. Some of the most common examples include **[6]** :

- Pasta.
- Crystallized sugar, which is obtained through evaporation.
- Fruit juices, which are prepared from a concentrate obtained by vaporization.
- Salt (from mining deposits), which is crushed, dissolved, purified, then drained and finally dried to become refined salt.
- Certain powdered products : cocoa, milk.

I.6.2. Wood Industry

Freshly cut and sawn wood has a high moisture content, making it unsuitable for immediate use. Without proper drying, the wood is prone to dimensional changes (shrinkage, swelling) and deformations (warping, cracking) during use. Drying is therefore an essential step to stabilize the material, ensure its durability, and allow its use under optimal conditions.

Figure I.1: *Wood drying.*

I.6.3 Food and Pharmaceutical Industries

Drying plays a crucial role in the preservation and effectiveness of many pharmaceutical and medicinal products. Certain medicinal plants used in the treatment of various diseases must be carefully dried to preserve their active compounds and prevent any degradation. Similarly, in the modern pharmaceutical industry, the drying of tablets, powders, or extracts occurs at various stages of production to ensure the drug's stability, concentration, and shelf life.

Figure I.2: *Drying of food and pharmaceutical products.*

I.7. Type of Drying

Solar energy drying is an economical and environmentally friendly method, particularly suited for processing agricultural products in small to medium quantities. It allows for the valorization of production surpluses while reducing post-harvest losses. This technique is still widely used, both at the household level and in small to medium-scale commercial operations. It is employed for drying various products such as fruits, vegetables, aromatic plants, food items, and even wood, thereby contributing to sustainable development and the local economy of rural communities. **[3]**

Solar radiation drying can be classified into two main categories:

- Direct, or open-air sun drying, the direct exposure to the sun
- Indirect solar drying or convective solar drying.

I.7.1. Direct solar drying

The direct solar drying technique involves spreading the product to be dried (Figure I.4) in a thin layer, if possible, over large open-air threshing surfaces, where it is left until it reaches the desired moisture content. From time to time during the day, the material must be turned to speed up drying and allow trapped moisture to escape. The drying surface is generally made of concrete-paved ground covered with polyethylene nets, but sensitive foods are placed on perforated trays. It is widely practiced for raisins, figs, and various fruits. As is evident, the drying rate is very low. Crops must remain outside for long periods, usually from 10 to 30 days, depending on their nature and the site's weather conditions.

Figure I.3: *Direct solar drying of seedless black Corinthian grapes on a concrete threshing floor in open air.*

I.7.2.Indirect Solar Drying

Indirect solar drying, also known as convective solar drying, uses solar collectors to heat air, which is then directed into a drying chamber. The products are not exposed directly to sunlight, which improves the sanitary quality of the drying process, reduces the loss of light-sensitive nutrients, and allows for better control of drying conditions (temperature, humidity, and airflow). **[2]**

I.8. Solar Dryer

I.8.1. Definition

Solar dryers are simple devices that collect solar radiation and convert it into thermal energy. This thermal energy is then transferred to the product for dehydration. Solar dryers can increase the dehydration temperature and reduce the relative humidity, thereby lowering the moisture content of the dried products. Unlike open sun, drying, solar dryers have a dedicated structure that regulates the dehydration process and protects the product from damage caused by dust, rain, and insects. **[7]**

I.8.2. Different Types of Solar Dryers

Solar dryers can generally be classified according to two main criteria:

- ✓ According to the mode of heat transfer: solar dryers are classified as *direct* (where

solar radiation reaches the product directly) and indirect (where the radiation heats an intermediate fluid, which in turn dries the product).

- ✓ According to the mode of air circulation: dryers are classified as passive, relying on

natural convection, and active, using forced ventilation powered by an auxiliary energy source (often photovoltaic solar or electric).

I.8.2.1. Direct Solar Dryer

In this type of solar dryer, a transparent cover is used to reduce heat losses, while also providing the product with effective protection against rain and dust. The necessary ventilation to remove the evaporated moisture is provided by upward air movement. A direct-type solar dryer is commonly used in areas that receive direct sunlight for extended periods during the day. **[8]**

***Figure I.4**: Direct solar dryer.*

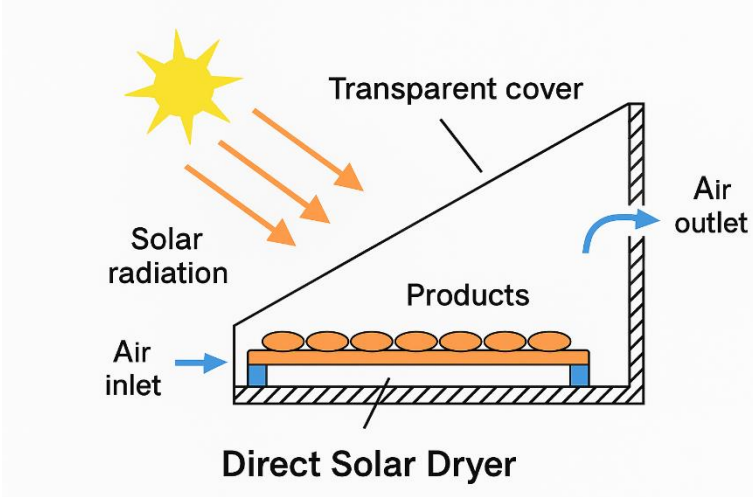

***Figure I.5**: Principle of a direct solar dryer.*

- **Advantages**

  - Better protection against dust, insects, animals, and rain compared to traditional drying.
  - No need for skilled labor.
  - Great design flexibility.

- **Disadvantages**

  - Quality degradation due to direct exposure to sunlight, including the destruction of vitamins A and C, wilting, and discoloration.
  - Fragility of polyethylene materials, which need to be replaced regularly.
  - Relatively high temperature inside the dryer, which, combined with sunlight exposure, contributes to the loss of nutrients. **[9]**

I.8.2.2 Indirect Solar Dryer

Indirect solar dryers differ from direct dryers in that the products to be dried are not exposed directly to solar radiation. Instead, these systems use convection processes either natural or forced—to circulate heated air around the products. Solar radiation is captured by a thermal collector, which heats a fluid (often air), and this heat is then indirectly transferred to the drying products. Moreover, the integration of solar energy with other sources, such as biomass, electricity, or other forms of thermal energy, enables these dryers to operate continuously even during low sunlight conditions, thereby improving their reliability and energy efficiency. **[10]**

Figure I.6: *Indirect solar dryer.*

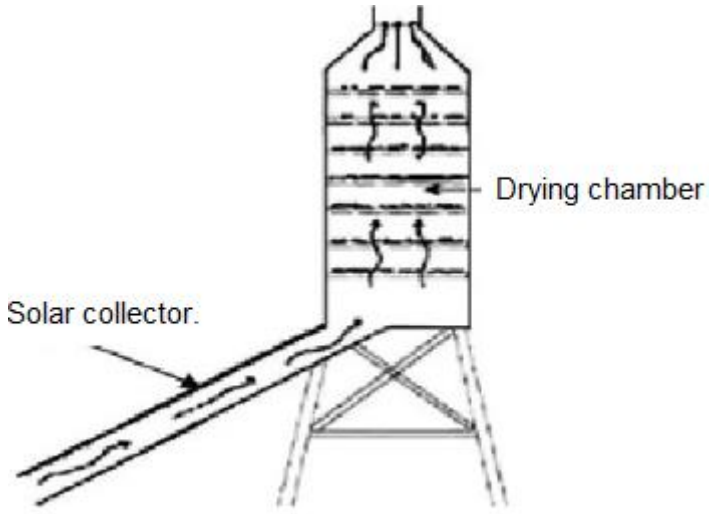

Figure I.7*: Schematic diagram of an indirect solar dryer.*

- **Advantages and Disadvantages**

o The drying rate is higher compared to direct solar drying.

o The final state of the product after drying can be scientifically controlled.

o Product losses are avoided under natural phenomena conditions.

o The required floor area is much smaller than that of direct solar drying for the same amount of material.

- Preserves the nutrient content of the product by avoiding direct exposure to solar radiation.

The main disadvantage of indirect solar drying is the high initial cost. **[11]**

I.8.2.3 Passive Solar Dryers (Natural Convection)

In this type of dryer, air circulates naturally through thermal convection (chimney effect). No mechanical device is used to force the movement of air. These dryers are simple, cost-effective, and suitable for small-scale agricultural production in rural areas. They can be easily built using low-cost, locally available materials, making them well-suited for small farms where raw construction materials such as wood are readily accessible. **[12]**

I.8.2.4. Active Solar Dryer (or Forced Convection Dryer)

Active solar drying systems are designed by integrating external means such as fans or blowers to move solar energy in the form of heated air from the collector area to the drying beds. Thus, all active solar dryers function as forced convection dryers. A typical active solar dryer uses solar energy solely as a heat source, while air circulation is provided by motor-driven fans or exhaust systems. These dryers are mainly used in large-scale commercial drying operations, often in combination with conventional fossil fuels, in order to better control the drying process by compensating for the effects of solar radiation fluctuations on drying air temperature **[13].**

Figure I.9 illustrates direct and indirect solar dryers operating under both natural and forced convection.

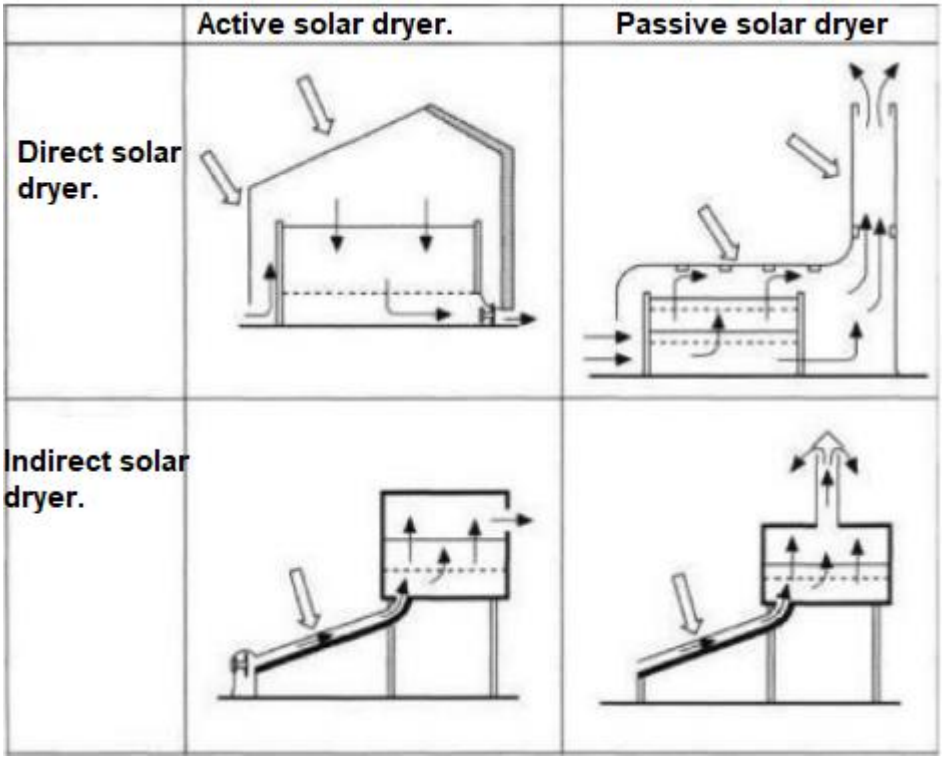

***Figure I.8**: Examples of direct and indirect solar dryers using natural convection and forced convection modes.*

I.8.2.5 Mixed solar dryer

Mixed-mode solar drying combines the principles of direct and indirect solar dryers. In this type of system, products are dried simultaneously by direct solar radiation and by hot air generated from a solar thermal collector. This dual heat source allows for better drying efficiency, especially compared to direct or indirect systems used separately. This mode thus offers improved performance in terms of both drying time and the quality of the final product. **[14]**

I.9. Literature Review

Several studies, both experimental and numerical, have focused on the operation and optimization of direct and indirect solar dryers (passive or active), highlighting their performance and limitations under various operating conditions.

Gbaha and **al. [15]** developed a natural convection direct-type solar dryer (Figure I.10), which they then evaluated experimentally by drying agricultural products such as cassava, banana, and mango slices. This simply designed dryer can be easily built by farmers using locally available materials. The results of the study showed that its thermal performance, in terms of heat and mass transfer, was significantly better than that achieved with traditional open-air solar drying.

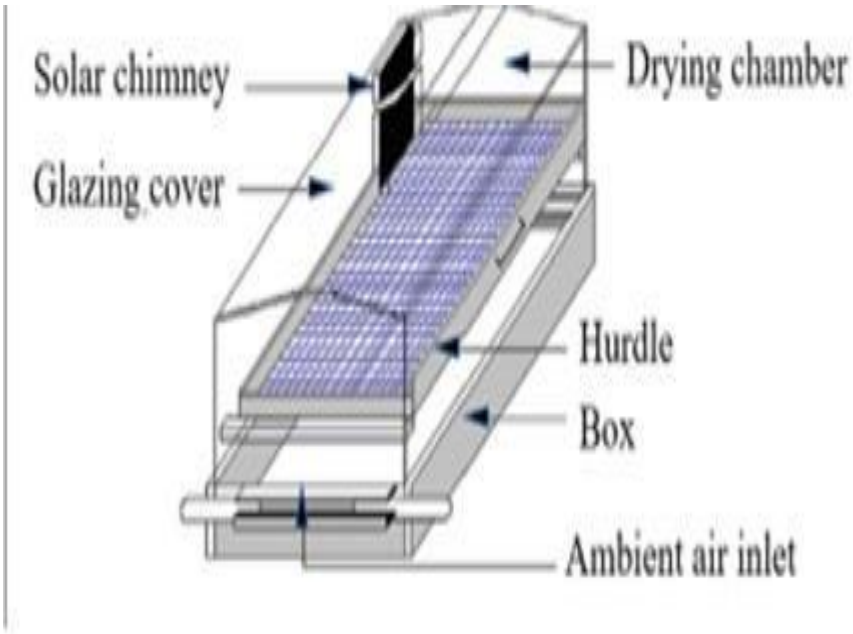

Figure I.9: *Direct solar dryer with a chimney*.

J.K. Afriyie and **al. [11]** evaluated a direct-mode solar dryer equipped with a chimney, designed for drying agricultural products. Their study focused on the impact of different roof inclination angles on drying performance. To this end, a laboratory prototype was built with roof angles of 81°, 64°, and 51° relative to the vertical plane. The drying chamber measured 440 mm in width, 420 mm in length, and 530 mm in total height. The base, made of 40 mm thick wood, was painted black to act as an absorbing surface for capturing solar radiation.

The results showed that this type of dryer is well suited to low-humidity air conditions. However, in the presence of highly humid air, preheating the air is necessary to maintain the efficiency of the process. The study also revealed that adding a properly sized solar chimney, combined with an optimal roof angle, can significantly improve the airflow rate and thus accelerate drying in a direct-mode system.

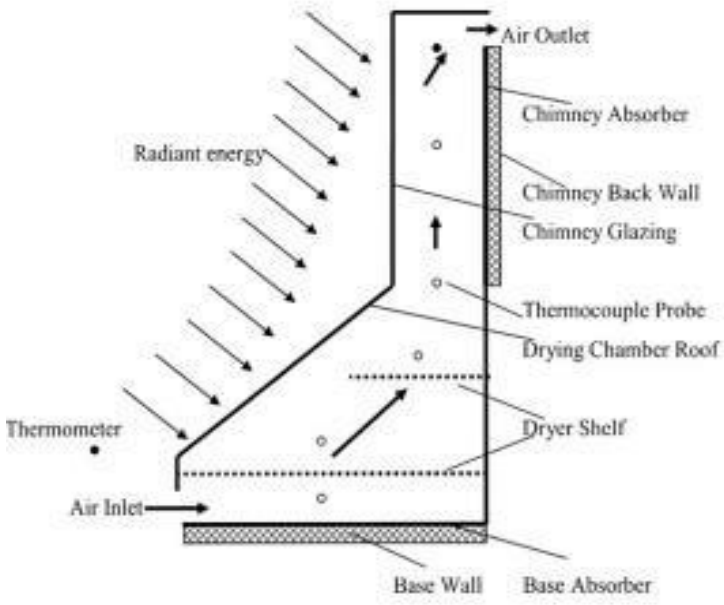

Figure I.10: *Functional architecture of a direct-mode solar dryer with a chimney.*

KANOUNE B. and **TRITIBA A. [16]** conducted an experimental study on a natural convection direct solar dryer consisting of a drying chamber and a chimney, incorporating two types of auxiliary energy sources to ensure continuous drying during the night or on cloudy days.

The first auxiliary source consists of geothermal hot water, coupled with a heat exchanger installed inside the drying chamber. The second auxiliary source is a solar water heater, also connected to the heat exchanger. The results showed that the integration of these auxiliary sources significantly improves the energy efficiency of the system, notably by extending the dryer's operation to up to 23 continuous hours. The study also highlighted a significant temperature difference between dryers with and without auxiliary systems, ranging from 12 to 36 °C on cloudy days.

It was concluded that using geothermal hot water as an auxiliary source offers superior energy performance, especially under unfavorable weather conditions (cloudy or nighttime), whether for daily operation or continuous day-and-night use.

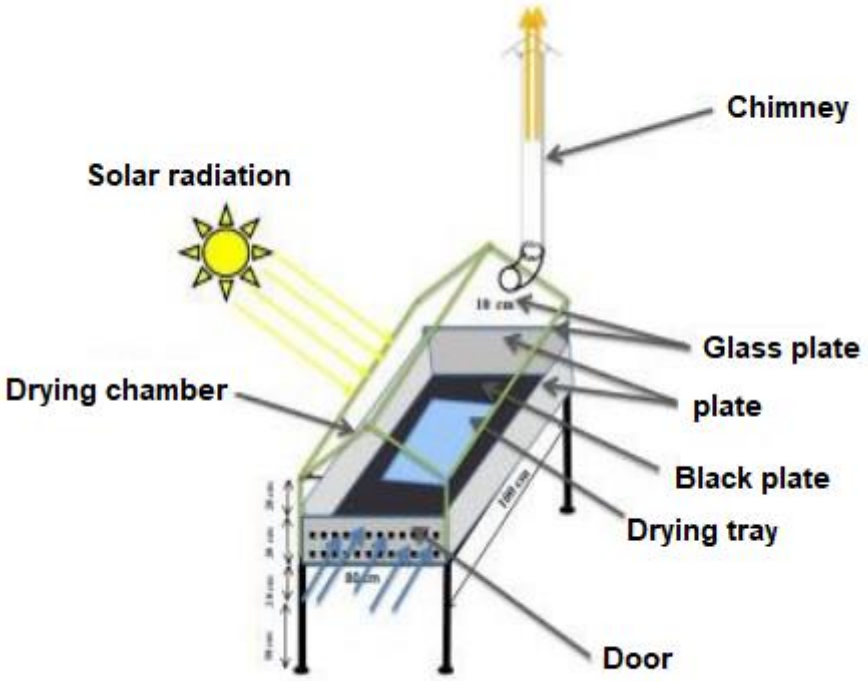

Figure I.11: *Diagram of a solar dryer.*

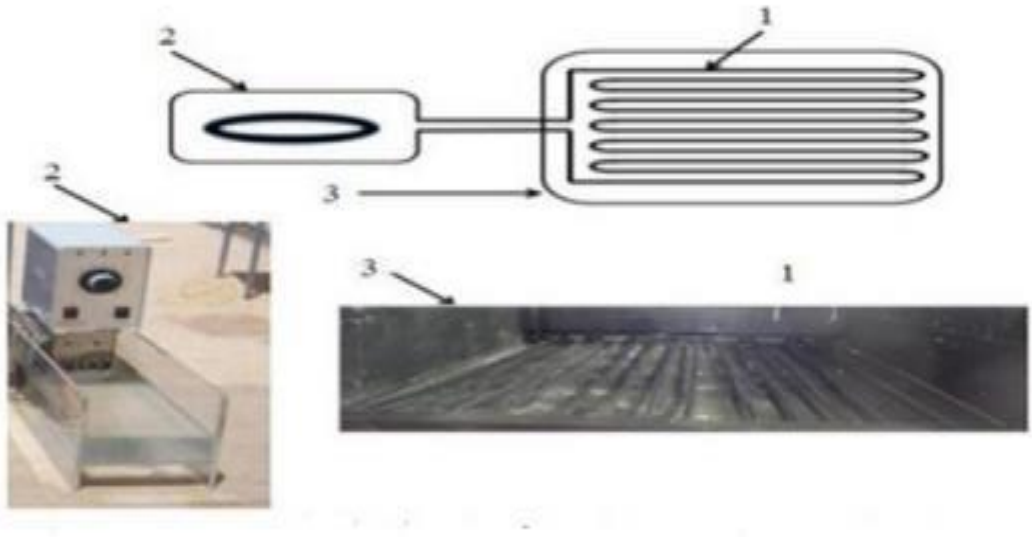

Figure I.12*: Representation of the auxiliary energy system installation.*

1-Heat exchanger2 – Hot water source3 – Drying chamber.

ZENGUI B. and **MANSOURI S. [17]** carried out a numerical study on a direct solar dryer, with and without the integration of a phase change material (PCM) layer, in order to store thermal energy in the form of latent heat. The simulations were performed using a

twodimensional unsteady model, based on the finite volume method, with the CFD Fluent software.

The results first validated the reliability of the numerical model by comparison with experimental data in the absence of PCM. The integration of a PCM layer then demonstrated a significant improvement in thermal behavior, particularly after sunset, by extending the drying process through the release of stored heat. The liquid PCM releases its heat to the absorber, thereby maintaining a useful temperature for the circulating heat transfer fluid.

Among the tested parameters, a PCM thickness of 4 cm made it possible to extend the operation of the dryer by approximately four additional hours after sunset. Furthermore, a PCM with a melting temperature of 326.5 K (53.5 °C) showed the best thermal performance. However, the study also pointed out that the efficiency of PCMs remains limited during low-sunlight days.

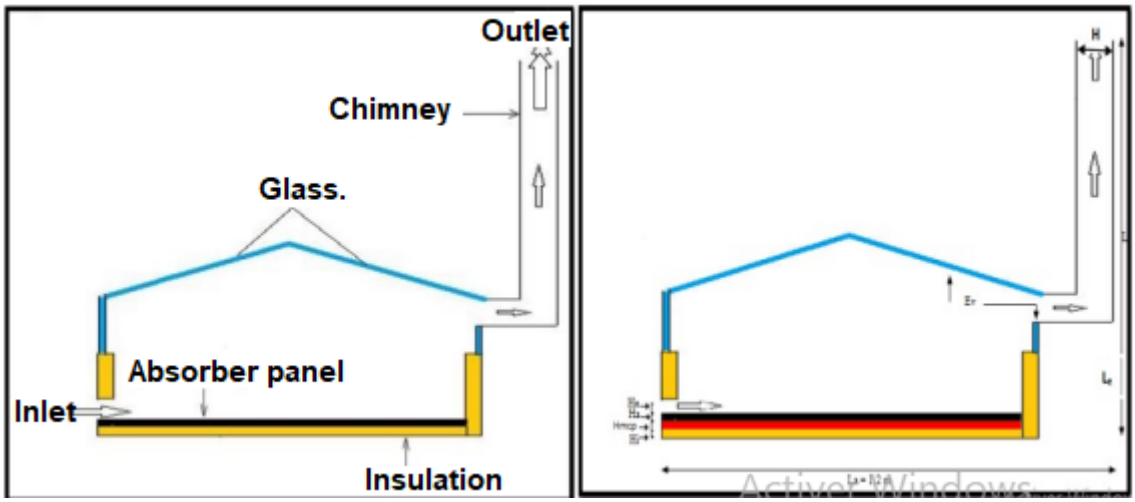

Figure I.13: Direct solar dryer without PCM and with PCM.

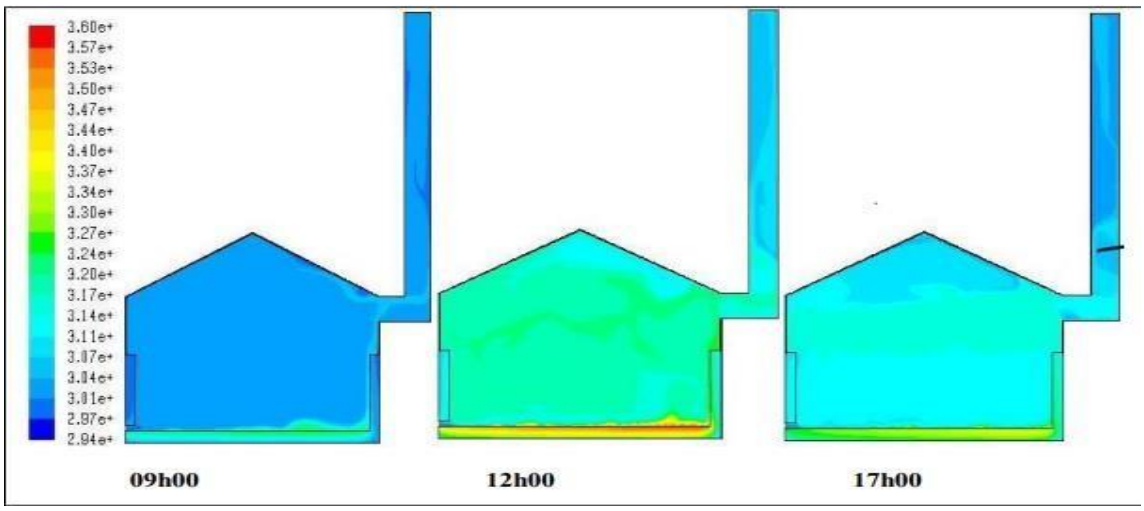

***Figure I.14**: Temperature distribution in the direct solar dryer without PCM.*

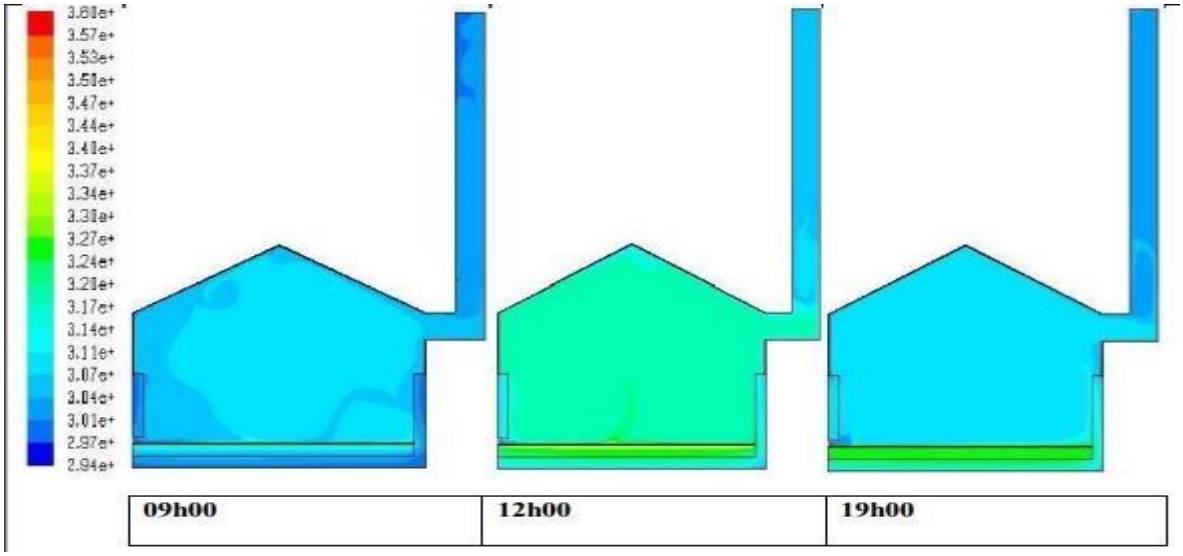

***Figure 15:** Temperature distribution in the direct solar dryer with PCM.*

Sari F. and **al. [18]** conducted an experimental study to evaluate the performance of an indirect solar dryer designed for drying cocoa beans. The system consisted of three main components:

- A drying chamber.
- A thermal solar collector.
- A thermal energy storage system with desiccant.

Two types of desiccant materials were used:

- Molecular sieve 13X (adsorbent).
- Calcium chloride ($CaCl_2$) (absorbent).

The experimental results showed that:

- The drying temperature reached between 40 and 54 °C, which is about 9 to 12 °C higher than the ambient temperature ideal for cocoa drying.
- In the absence of sunlight, the air inside remained drier than the ambient air, thanks to the effect of the desiccants.

Method	**Time**
Intermittent direct solar drying	55 hours
Dryer with adsorbent desiccant (13X sieve)	41 hours
Dryer with absorbent desiccant ($CaCl_2$)	30 hours

They also concluded that integrating desiccant-based thermal storage into a solar dryer makes solar drying more efficient in terms of drying time and specific energy consumption.

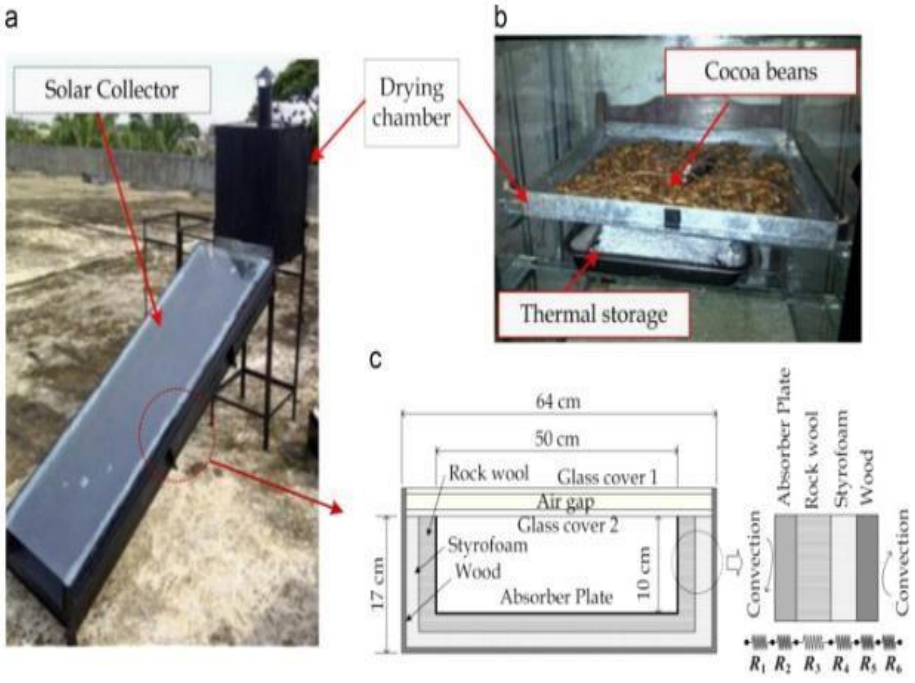

***Figure I.16**: (a) Experimental solar dryer, (b) Drying tray, (c) Thermal resistance analogy of the solar collector envelope.*

SHAMEKHI A. and **al. [19]** studied the thin-layer drying behavior of lemon balm leaves in an indirect-mode forced convection solar dryer. The air solar collector featured an innovative

counter-flow double-pass configuration with a fixed bed made of wire mesh, designed to enhance the energy gain of the heated air. The system consisted of a double-pass air collector with a fixed wire mesh bed connected to a drying chamber. The thermal efficiency of the collector was determined under realistic conditions, with solar irradiance ranging from 600 to 900 W/m², ambient temperature from 22 °C to 25 °C, and outlet air temperature from 38 °C to 68 °C.

They concluded that increasing the airflow rate from 0.006125 m³/s to 0.01734 m³/s improved the thermal efficiency of the collector by approximately 20%. However, a further increase in the airflow rate to 0.034378 m³/s had a negative effect on this efficiency. Drying experiments were carried out on lemon balm leaves with an initial moisture content of 80% (wet basis), which was reduced to a final moisture content of 10%.

Figure I.17: *(a) Photos of the tested solar dryer, (b) Final dried product from each trial.*

AMEUR K. and BENOSMANE I. [20] conducted an experimental study aimed at analyzing the thermal behavior of a forced convection solar dryer, as well as monitoring the drying kinetics of various agri-food products. Their work focused particularly on the effect of integrating fins on the absorber and narrowing the air duct within the solar collector. These modifications were evaluated in terms of the thermal performance of the dryer and their impact on the drying kinetics of thin slices of bell pepper, tomato, strawberry, and apple.

***Figure I.18**: Prototype of the constructed solar dryer.*

They concluded that using a simple absorber resulted in a temperature difference of 29 °C between the absorber and the air at the collector outlet. The temperature difference between the inlet and outlet of the collector was 13.5 °C. The bell peppers showed a mass loss of approximately 86%, 83%, and 84% for trays 1, 2, and 3 respectively, and the moisture content was reduced to 9% over a 15-hour period. After the integration of fins, the maximum temperature difference between the absorber and the outlet air was reduced by 24.8%, while the difference between the inlet and outlet air was increased by 21.5%. As a result, the drying time was reduced by 10%.

LOUAZENE A. and BOUHNIK A. [21] carried out a numerical study on improving the thermal performance of an indirect solar dryer with natural ventilation, by evaluating the effect of integrating phase change materials (PCM) into the collector, the chimney, or both.
Using a two-dimensional unsteady model based on the finite volume method with CFD Fluent, they showed that the addition of a solar chimney particularly with a 3 cm air gap offset toward the north—significantly enhances thermal performance. The integration of paraffin into the collector and chimney extends the efficiency of the dryer after sunset, maintaining stable natural ventilation between 0.7 and 0.9 m/s for an additional two hours.

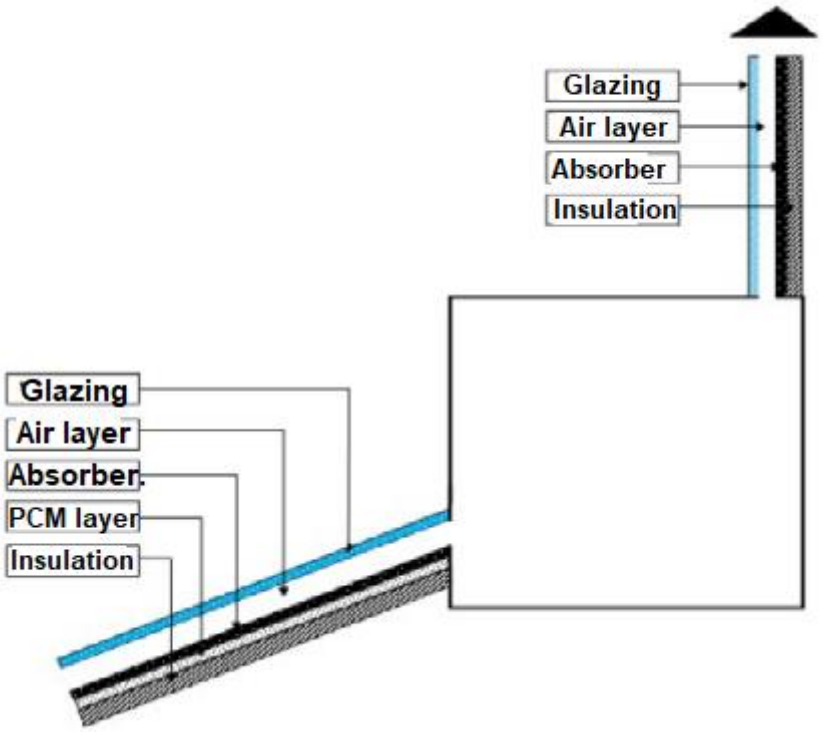

Figure I.19: *Schematic diagram of the dryer with PCM integration in the collector.*

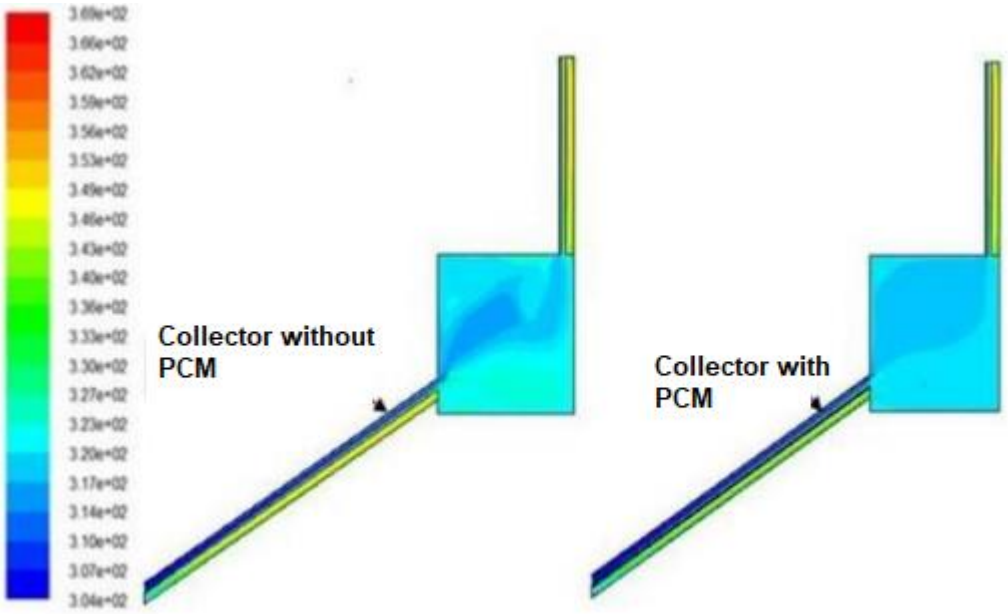

Figure I.20*: Temperature field inside the dryer with and without PCM in the collector.*

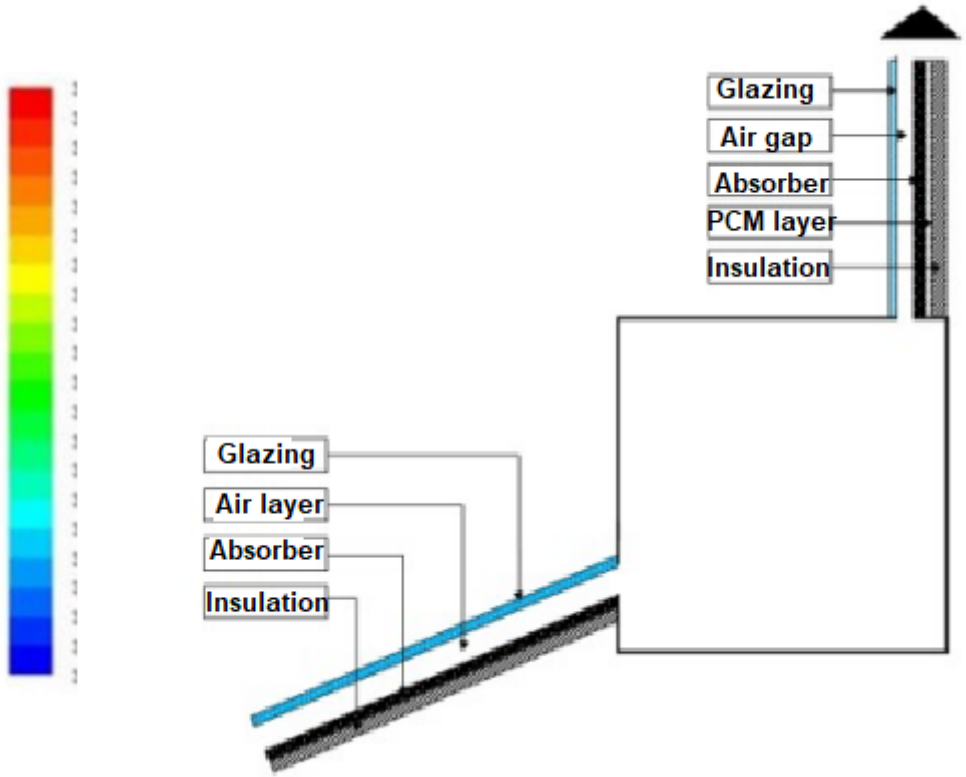

***Figure I.21**: Schematic diagram of the dryer with PCM integration in the solar chimney.*

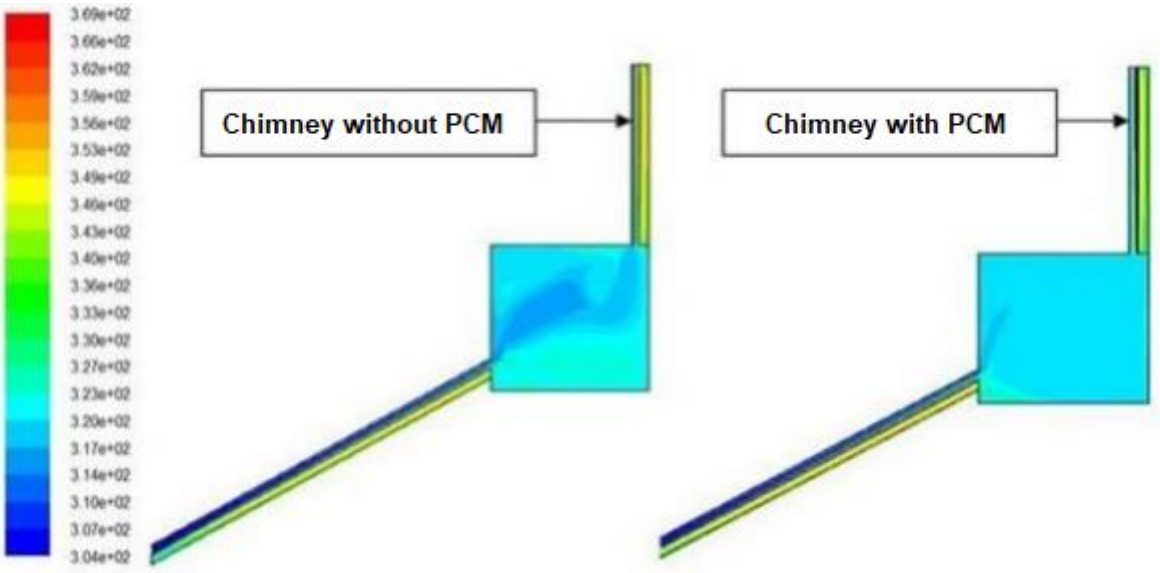

***Figure I.22**: Temperature field inside the dryer with and without PCM in the solar chimney.*

Khaldi S. [2] conducted a numerical study on a natural convection indirect solar dryer designed for drying figs. The analyzed system includes a drying chamber coupled with an inverted absorber and a solar chimney. The simulations assessed the impact of chimney configuration and the size of the air inlet opening on thermal and flow fields.

The study also investigated the effect of adding a gravel bed, modeled as a porous medium, for thermal storage within the drying chamber. Finally, the introduction of a second air inlet was proposed to improve thermal homogeneity between the drying shelves and to optimize drying uniformity.

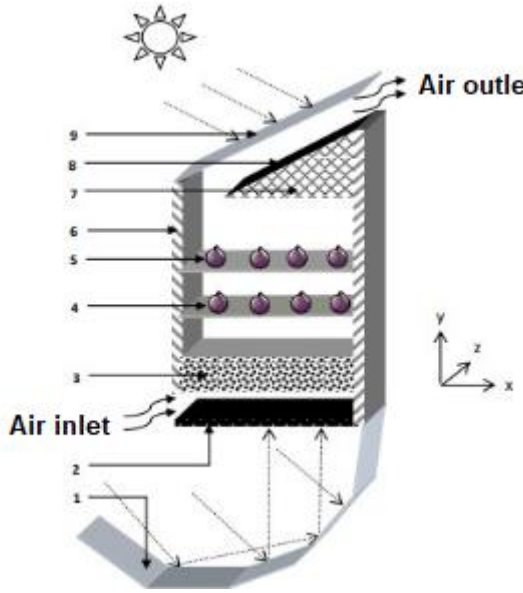

***Figure I.23**: Schematic diagram of the solar dryer integrating a thermal bed.*

The study concludes that the addition of a solar chimney, even without thermal storage, increases the air mass flow rate and ventilation rate by up to 5%. However, integrating a thermal storage material into the chimney significantly improves the mass flow rate, reaching an increase of 32% during nighttime. Gradually enlarging the air inlet opening (from 0.04 m to 0.10 m) also facilitates air extraction, resulting in an increase in airflow between 13% and 18.69%, but at the cost of a product temperature drop of up to 14.89%. Moreover, introducing a thermal gravel bed with a thickness of 0.05 m reduces the mass flow rate by up to 25%, while a thickness of 0.15 m optimizes thermal storage and extends the dryer's operating time by 44.59%.

Finally, the porosity of the bed plays a crucial role: high porosity increases the product's maximum temperature, whereas low porosity promotes prolonged nighttime operation.

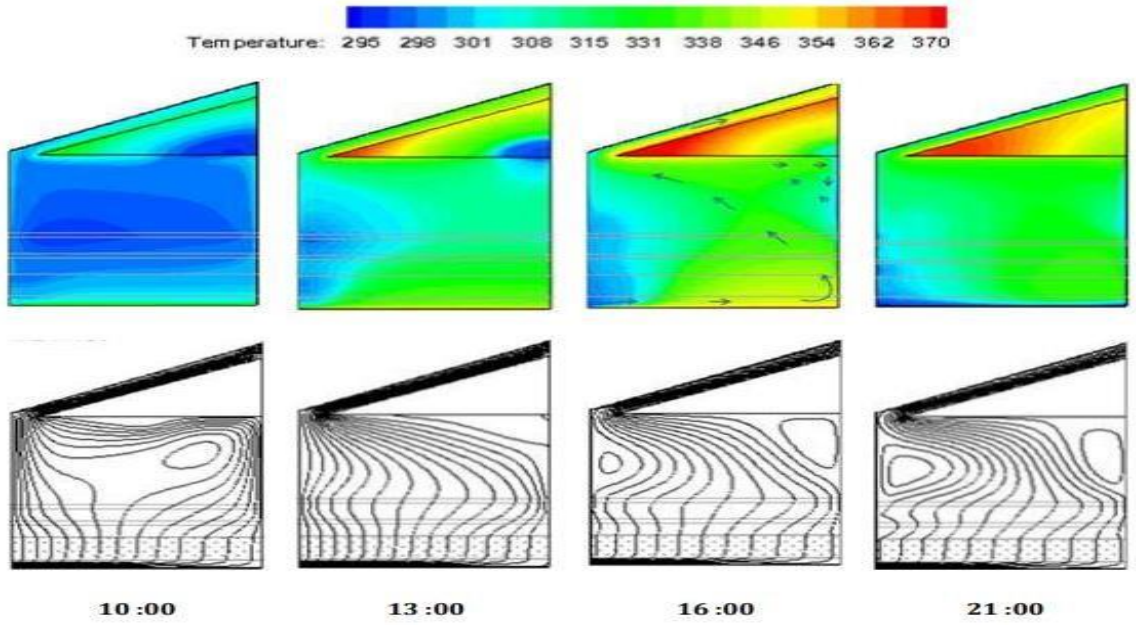

***Figure I.24**: Temperature contours and streamlines inside the solar dryer with thermal bed.*

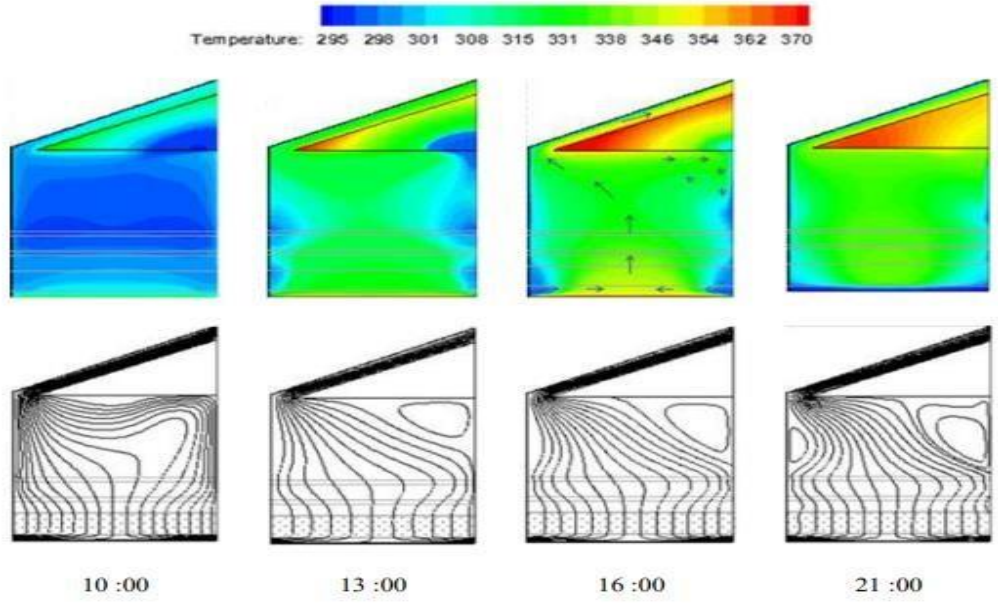

***Figure I.25**: Temperature contours and streamlines inside the solar dryer with two air inlets.*

UGWUOKE I. C. and **al. [22]** developed a domestic mixed-mode solar dryer in which slices of chili pepper, okra, and yam were simultaneously dried by both direct radiation through the transparent glass roof of the drying chamber and by heated air from the solar collector. The dryer consisted of a solar collector, a desiccant chamber, and a drying chamber containing a rack with three trays.

They concluded that the maximum temperatures reached during the tests were 69 °C for the solar collector and 55 °C for the drying chamber, with a corresponding ambient temperature of 39 °C.

A mass of water removed was 43 g, 136 g, and 255 g respectively for chili pepper, okra, and yam slices using the passive solar dryer, compared to 39 g, 126 g, and 218 g respectively by open sun drying, indicating differences of 4 g, 10 g, and 37 g for chili pepper, okra, and yam respectively.

The rapid drying rate obtained using this dryer demonstrates its ability to dry food items quickly to an acceptable moisture level.

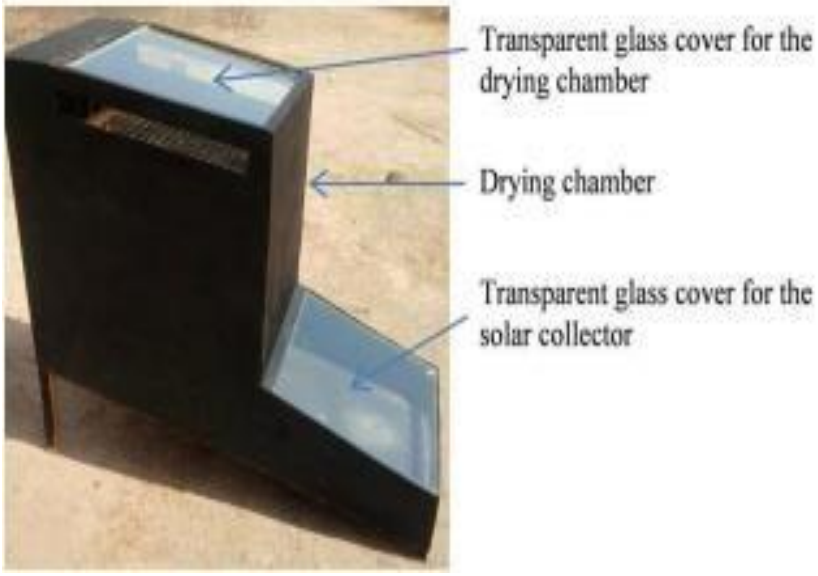

***Figure I.26**: Mixed-mode solar dryer.*

I.10. Conclusion

Drying remains a crucial step in the processing and preservation of many products. Solar dryers, as simple, cost-effective, and environmentally friendly systems, offer a promising solution to current energy challenges. The literature review presented in this chapter has highlighted the different dryer designs, their performance, and the improvements introduced through research.

Chapter II

Physical Model, Mathematical Formulation, and Numerical Resolution.

II.1. Introduction

This chapter presents a numerical simulation carried out using the ANSYS Fluent 19 software, validated with experimental data previously collected at the University of Tlemcen (ABOU BEKR BELKAID), within the Applied Energetics and Thermal Research Laboratory No. 63 (ETAP) **[20]**. The study focuses on the analysis of the thermodynamic behavior of a compact indirect solar dryer, with the aim of characterizing the heat transfer mechanisms and airflow dynamics within the system.

The examined setup consists of a thermal solar collector coupled to an insulated drying chamber, where heat transfer occurs through a flow of heated air, without direct exposure of the products to solar radiation. The collector, tilted at 45°, is equipped with a black-painted steel absorber to maximize radiation absorption, thereby increasing the air temperature. A glass glazing ensures the transmission of solar radiation inside the collector. A fan is positioned at the inlet of the solar collector to ensure the controlled admission of air at a fixed velocity, thus maintaining continuous circulation toward the drying chamber and establishing a forced convection regime within the system.

Figure II.1: *Prototype of the constructed solar dryer*

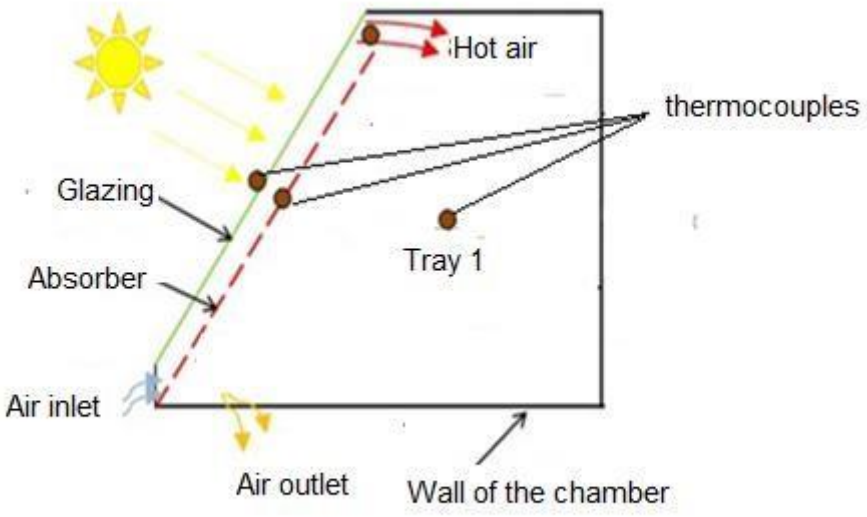

Figure II.2: *Schematic diagram of the solar dryer*

II.2. Physical model

The studied domain corresponds to a solar dryer equipped with a flat, inclined, rectangular-shaped collector, measuring 78 cm in length and 50 cm in width. This collector includes an absorber and a glass cover. Ambient air, with a temperature that varies over time and an assumed uniform velocity, enters the drying chamber by passing through the inclined collector, flowing between the absorber and the glazing. The latter receives solar radiation, which also varies with time. The heated air is then discharged through the bottom wall of the chamber. The lateral walls are considered thermally insulated. The adopted coordinate system and the physical model of the solar dryer are presented in Figure III.1 and Table III.1 **[20].**

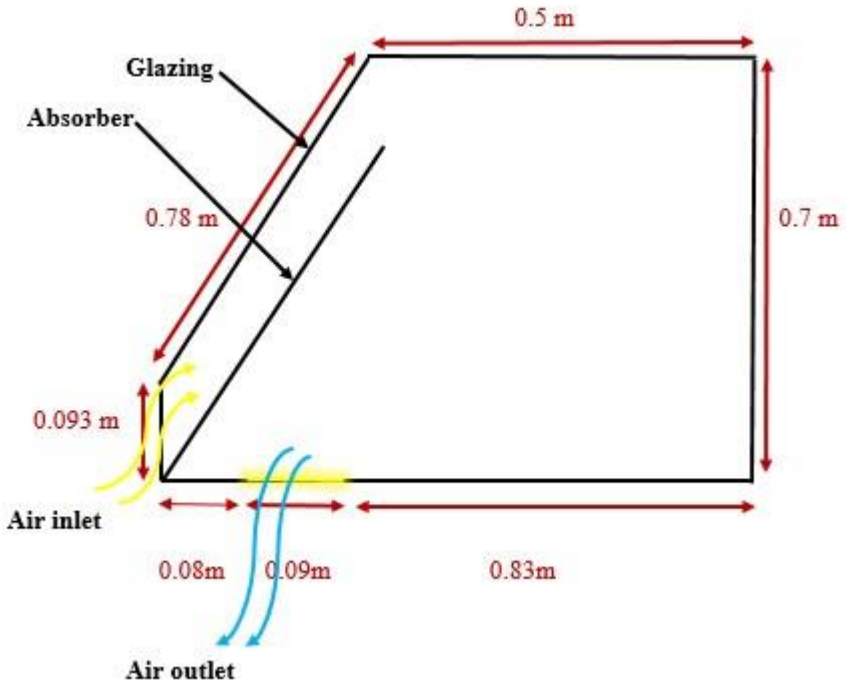

Figure II.3: Diagram of the physical model of an indirect solar dryer

Table II.1: Dimensions of the glazing and absorber of the solar dryer

	Thickness (m)
Glazing	0.002
Absorber	0.005

Table II.2: Thermophysical Properties of the Solar Dryer

	ρ (kg/m³)	**Cp (J/kg.k)**	**ƛ (w/m.k)**	**μ* 10-5 (kg/m.s)**	**α**	**τ**	**E**
Air (fluid)	1.225	1006.43	0.0242	1.7894	/	/	/
Glass (solid)	2530	840	1.05	/	0.06	0.95	0.5
Steel (solid)	7870	447	80.2	/	0.95	/	0.88

II.3. Simplifying hypotheses

The formulation of the studied problem is based on a set of simplifying assumptions, particularly concerning the geometry and type of flow. In order to achieve a solution that is both simple and realistic, the following assumptions were made:

- The flow is assumed to be two-dimensional and incompressible.
- The flow is unsteady and laminar.
- The fluid is assumed to be incompressible, viscous, and Newtonian.
- The thermophysical properties (ρ, Cp, λ, μ) of the fluid (air) and the solid components of the dryer (absorber and glazing) are considered constant.
- The airflow follows the Boussinesq approximation.

II.4. Mathematical Model

The equations that describe the motion of air in the drying system are based on the laws of conservation of mass, momentum, and energy. The equations can be formulated as follows :

II.4.1. In the Air

Continuity Equation :

$$\frac{\partial u}{\partial x} + \frac{\partial v}{\partial y} = 0 \qquad \text{II.1}$$

u and v represent the components of the fluid velocity along the x and y-axes, respectively.

Momentum equation :

Along the x-axis

$$\rho\left(\frac{\partial u}{\partial t} + u\frac{\partial u}{\partial x} + v\frac{\partial u}{\partial y}\right) = -\frac{\partial P}{\partial x} + \mu\left(\frac{\partial^2 u}{\partial x^2} + \frac{\partial^2 v}{\partial y^2}\right) \qquad \text{II.2}$$

Along the y-axis:

$$\rho\left(\frac{\partial v}{\partial t} + u\frac{\partial (v)}{\partial x} + v\frac{\partial (v)}{\partial y}\right) = \frac{-\partial p}{\partial y} + \mu\left(\frac{\partial^2 u}{\partial x^2} + \frac{\partial^2 v}{\partial y^2}\right) + \rho g\beta(T-T_0) \qquad \text{II.3}$$

Energy Equation :

$$\rho C_p \left(\frac{\partial T}{\partial t} + u\frac{\partial T}{\partial x} + v\frac{\partial T}{\partial y}\right) = \lambda\left(\frac{\partial^2 T}{\partial x^2} + \frac{\partial^2 T}{\partial y^2}\right) \quad \text{II.4}$$

II.4.2. Energy conservation equation in the absorber and glazing

With regard to heat transfer in solid media (absorbers, glazing, insulation, granite), the governing equation is written as:

- **Absorber**

$$\frac{\partial Ta}{\partial t} = \frac{\lambda a}{\rho a.Cpa}\left(\frac{\partial^2 Ta}{\partial x^2} + \frac{\partial^2 Ta}{\partial y^2}\right) \quad \text{II.5}$$

Where:

T_a : Temperature in the absorber [K] λ_a :Thermal

conductivity of the absorber [w/mk].

ρ_a : Density of the absorber [Kg/m^3].

C_{pa} : Specific heat capacity [J/Kg.K].

- **Glazing**

$$\frac{\partial Tv}{\partial t} = \frac{\lambda g}{\rho g.Cpg}\left(\frac{\partial^2 Tv}{\partial x^2} + \frac{\partial^2 Tv}{\partial y^2}\right) \quad \text{II.6}$$

Where:

T_g: temperature inside the glazing [K].

λ_g : thermal conductivity of the glazing [w/mk].

ρ_g : density of the glazing material [kg/m^3].

C_{pg} = specific heat capacity of the glazing material [J/kgk]

II.5. Initial and boundary conditions

II.5.1.Equation of ambient temperature variation as a function of time:

Figure II.4 illustrates the variation of ambient temperature as a function of time during the first and second sunny days (from 9h30 to 17h00). The results used were previously obtained in earlier work **[20]**. The mathematical expression approximating the experimental evolution was developed using OriginPro software

$$T_a\,(t) = 20 + 9\cos\left(\frac{\pi}{11}\,(t - 14)\right) \qquad \text{II.7}$$

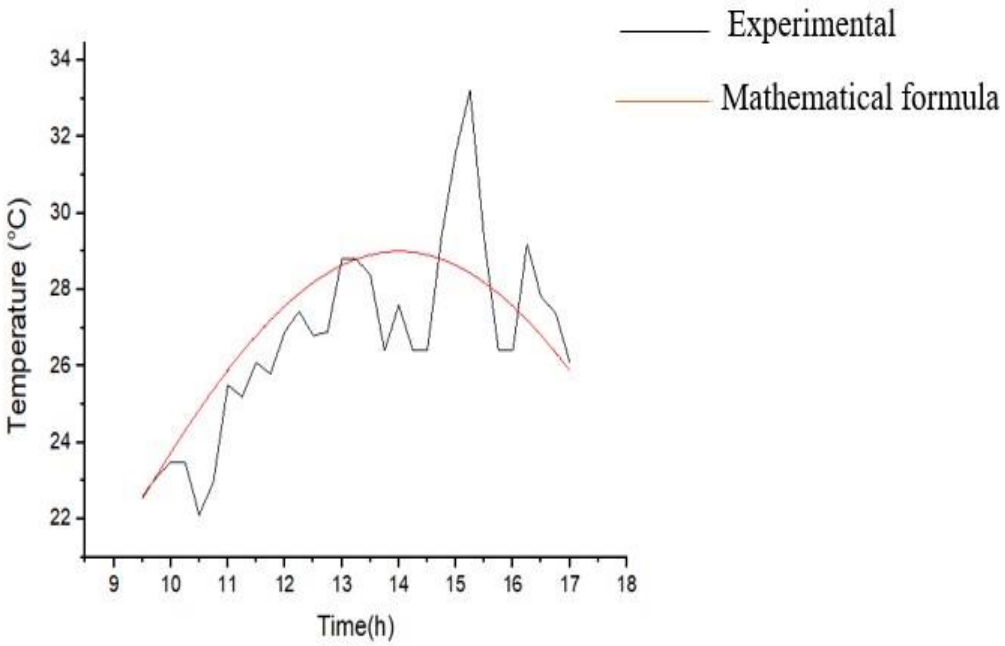

Figure II.4: Temporal evolution of ambient air temperature

II.5.2. Equation of global solar radiation variation as a function of time

Figure II.5 illustrates the variation of global solar radiation as a function of time during a sunny day (from 9h30 to 17h00). The results used were previously obtained in earlier work **[20].** The mathematical expression approximating the experimental trend was developed using OriginPro software:

$$G\,(t) = 1091\,\sin\left(\frac{t-7.9}{18.07-7.9}\,\pi\right) \qquad \text{II.8}$$

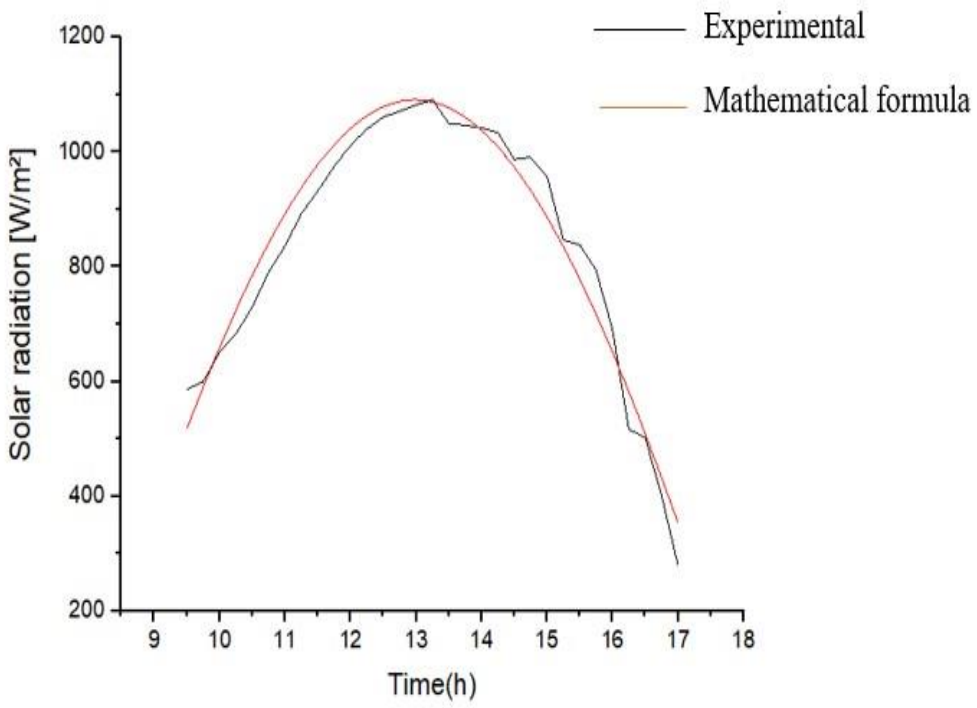

Figure II. 5: Temporal evolution of solar radiation

The solar collector of the dryer includes two optically active elements: the glazing, which allows part of the radiation to pass through, and the absorber, which captures the useful energy. Their optical properties determine the amount of heat transferred to the circulating air. The model takes into account the phenomena of transmission, absorption, and radiative emission.

- **Glazing**

The glazing acts as an interface between the outside environment and the absorber. It transmits part of the direct and diffuse solar radiation, but also generates losses through radiation and convection.

The transmitted flux through the glazing is given by :

$$Q_{transmis} = \alpha_v.G/e_v \qquad [W/m^3] \qquad II.9$$

Where:

α_v: absorption coefficient of the glazing.

G: incident global solar radiation [W/m²].

e_v: thickness of the glazing [m].

- **Absorber :**

The absorber is the black surface that captures the radiation transmitted through the glazing.

The absorbed energy flux is modeled by:

$$Q_{abs} = \alpha a.\tau v.\ G/e_a \qquad [W/m^3] \qquad \text{II.10}$$

Where:

α_a: absorption coefficient of the absorber plate.

τ_v: transmittance of the glazing,

G: global incident solar radiation [W/m²].

e_a: thickness of the absorber [m].

II.5.3. Initial Condition

In this study, the following assumptions are made for the initial conditions :

- At the initial moment, the entire dryer is assumed to be at ambient temperature.
- An airflow is already established at the inlet with a constant velocity.
- Initial air temperature : $T(t=0) = 295.6$ K (22°C)
- Initial air velocity : $V(t=0) = V_o = 0.55$ m/s (magnitude velocity)

II.5.4. Boundary Conditions

The boundary conditions were defined as follows:

- **Air inlet:** velocity inlet type condition, with ambient temperature varying over time.
- **Air outlet:** Pressure outlet condition type at atmospheric pressure.

The outer walls of the dryer are assumed to be insulated $\frac{\partial T}{\partial n} = 0$ (n denotes the normal to the surface).

- A no-slip condition (Wall type) is also imposed (zero velocities at the wall): u = v = 0.

II.6. Simulation using FLUENT

ANSYS Fluent 19 is a software used to solve and simulate problems related to fluid mechanics and heat transfer using the finite volume method.

In ANSYS Fluent 19, the model was defined according to the previously stated assumptions. To perform the simulation with this software, the solution parameters must be described as follows **[3]**:

II.6.1. Geometry

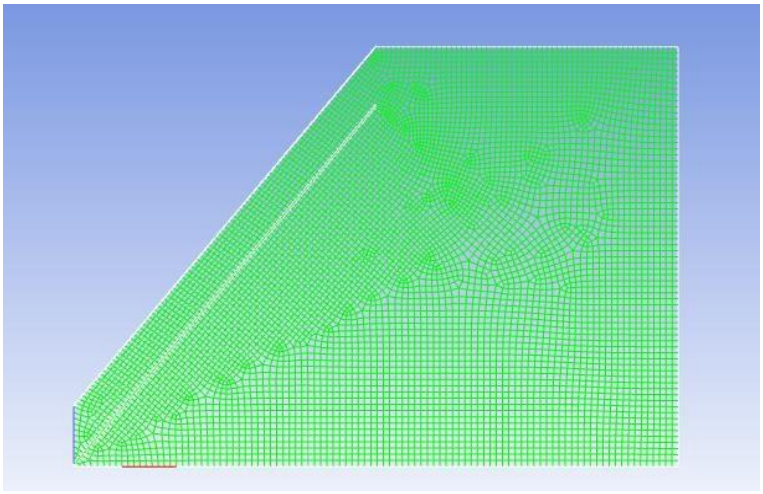

Figure II.6: Geometry of the Solar Dryer Modeled in ANSYS Fluent 19

II.6.2 Choice of solver type:

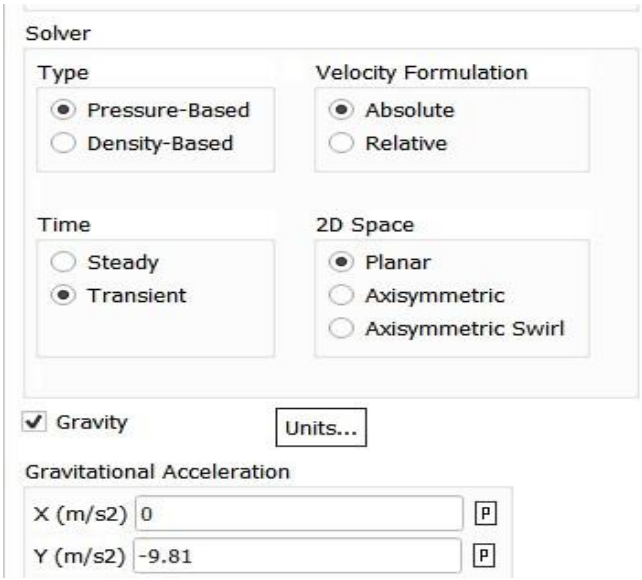

Figure II.7: General solver configuration in ANSYS Fluent

II.6.3 Choice of material :

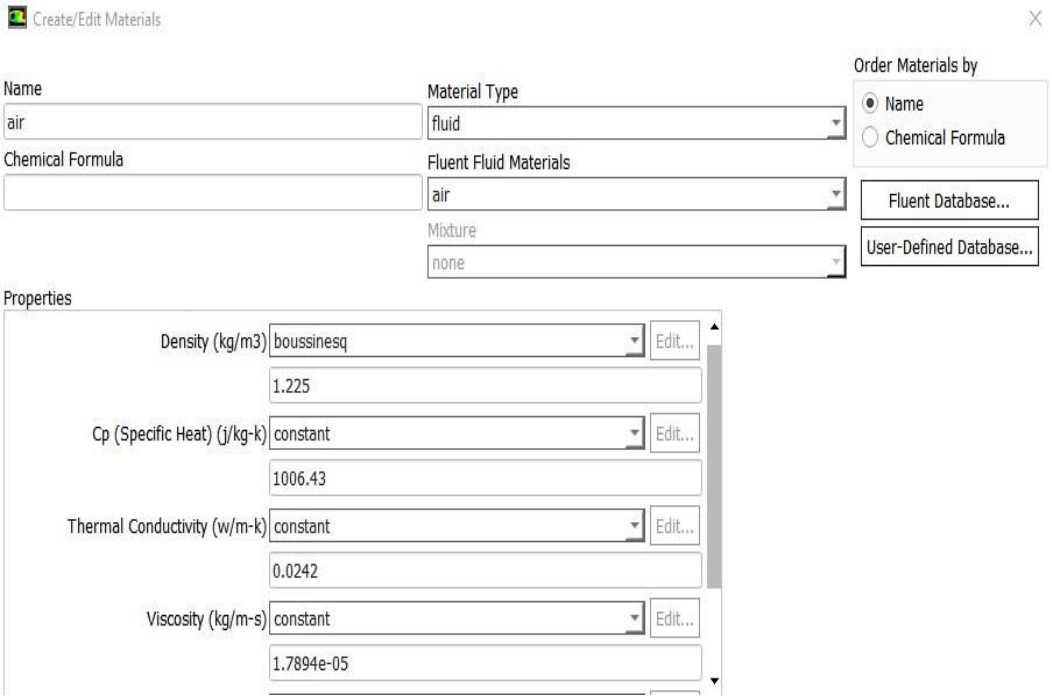

Figure II.8: Definition of the thermophysical properties of air in ANSYS Fluent

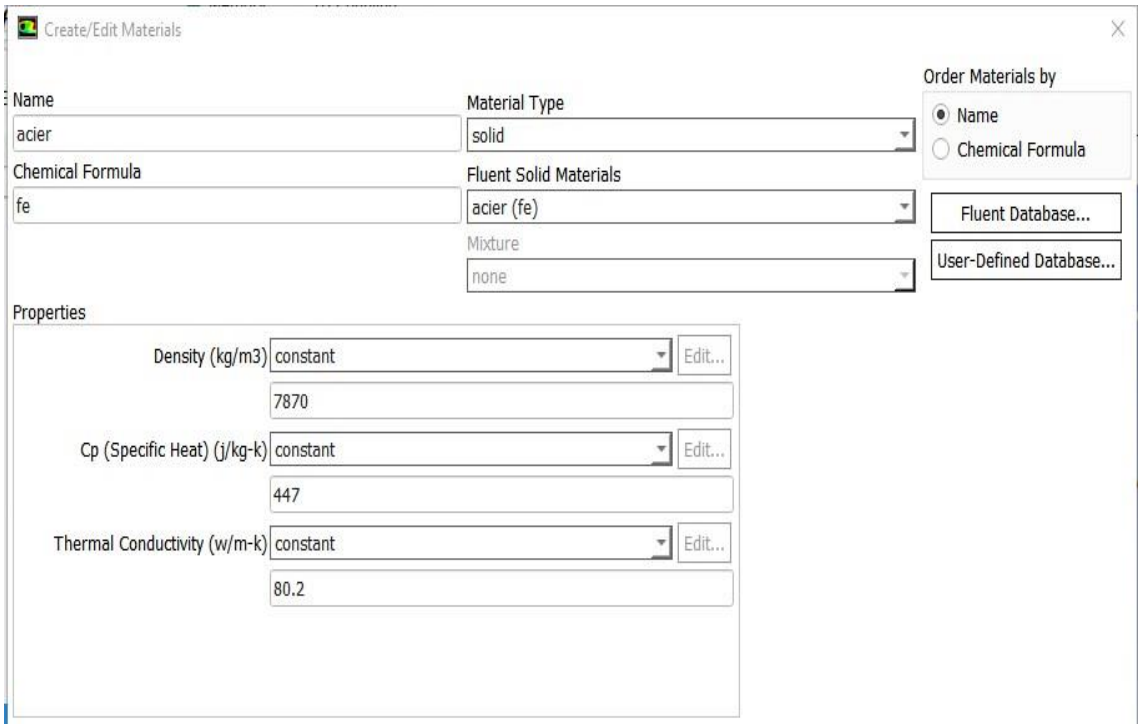

Figure II.9: Definition of the thermophysical properties of steel in ANSYS Fluent

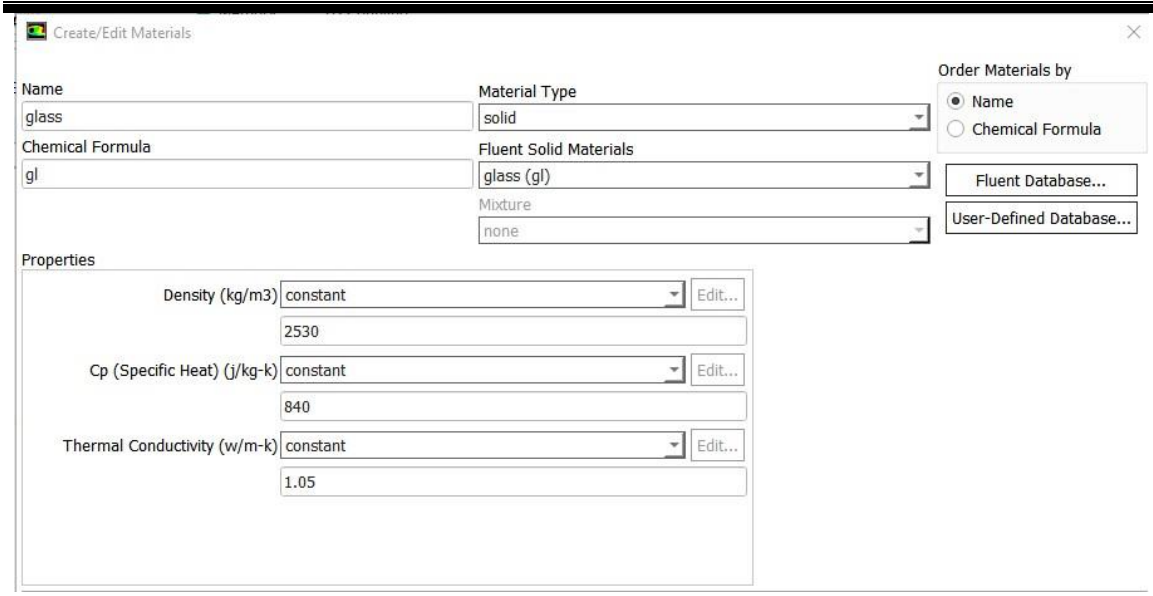

Figure II.10: Definition of the thermophysical properties of glazing in ANSYS Fluent

II.6.4. Solver Controls:

Unsteady calculation parameters:

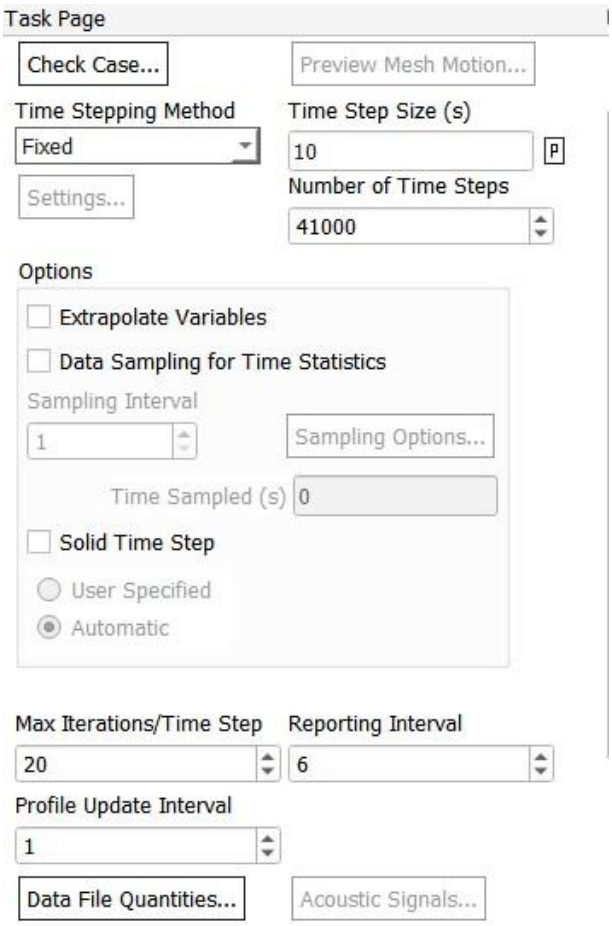

Figure II.11: Transient calculation control parameters

II.6.5. Pressure-Velocity Coupling :

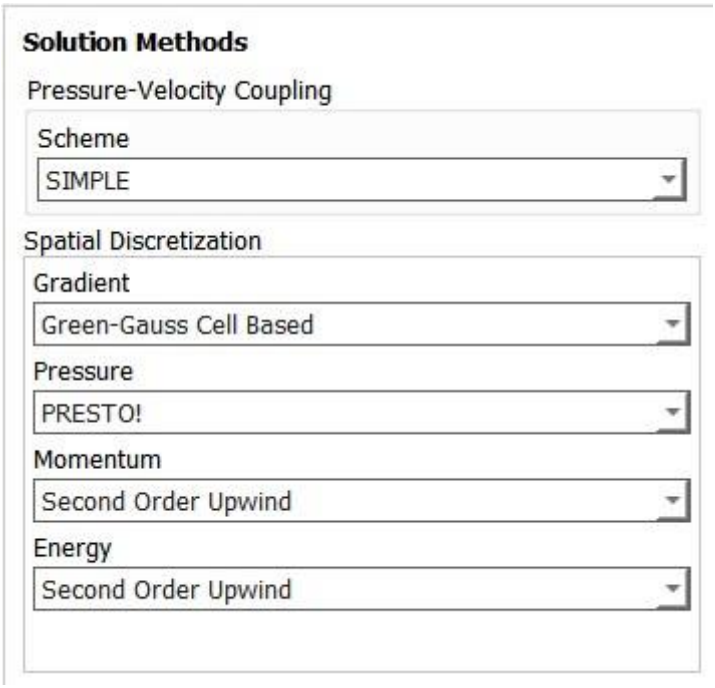

Figure II.12: Selection of the pressure-velocity coupling scheme in ANSYS Fluent

II.7. Mesh and Time Step test

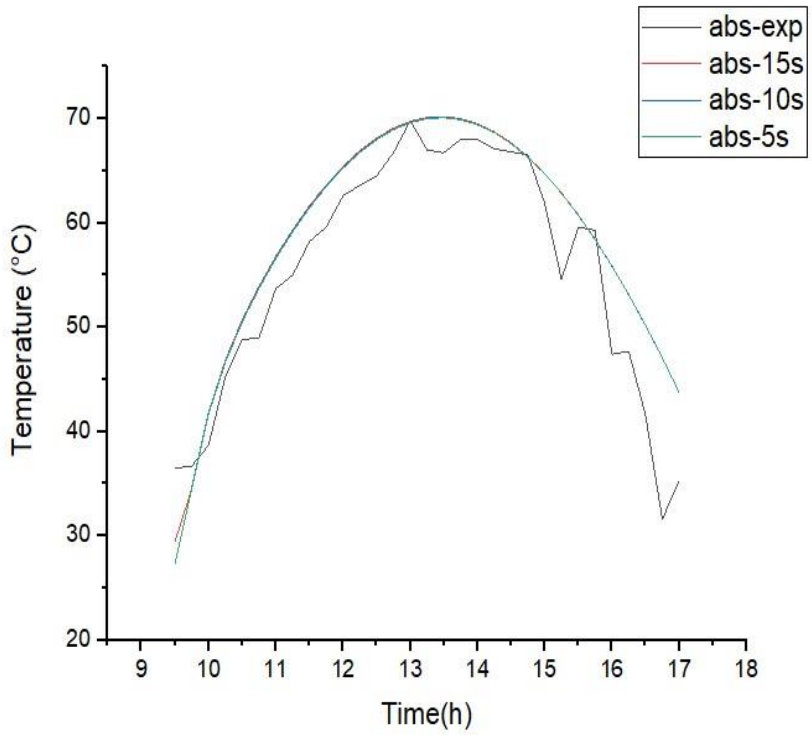

Figure II.13: Comparison of Absorber Temperature Over Time for Different Time Steps (dt = 5s, 10s, 15s) with Experimental Data

This graph shows the evolution of the absorber temperature throughout the day, comparing experimental data (abs-exp) with numerical results obtained using different time steps: 5 seconds, 10 seconds, and 15 seconds. Among the simulations, all three time steps (5s, 10s, and 15s) provide results that generally match well with the experimental data.

The table below presents the characteristics of the meshes used.

Table II. 3: Characteristics of the Meshes Used

Mesh size	**1**	**2**	**3**
Number of nodes	7769	5585	9698

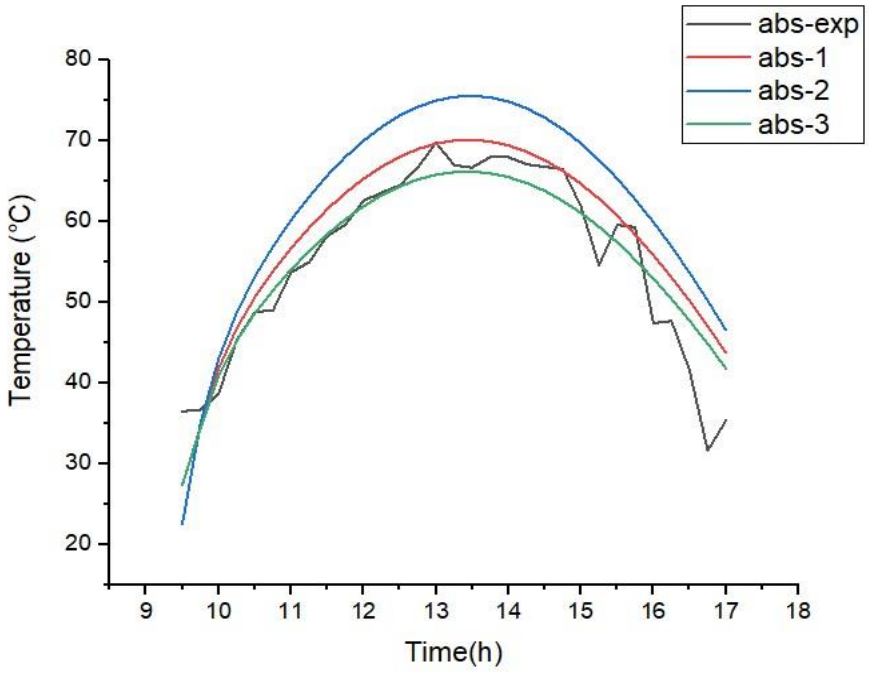

Figure II.14: Comparison of absorber temperatures for different mesh configurations and experimental data

Figure II.14 presents a comparison between the experimental absorber temperature and the simulated temperatures obtained using three different meshes: abs-1 (mesh with 7769 nodes), abs-2 (mesh with 5585 nodes), and abs-3 (mesh with 9698 nodes). It can be observed that the three numerical curves generally follow the same trend as the experimental data, with a gradual increase in temperature reaching a peak around 13h.–14h., followed by a decrease. Among the three meshes, the finest mesh (abs-3 with 9698 nodes) provides results that are closer to the

experimental data. On the other hand, the coarsest mesh (abs-2, 5585 nodes) overestimates the maximum temperature, while the intermediate mesh (abs-1, 7769 nodes) offers a reasonable compromise in terms of accuracy.

II.8. Conclusion

This chapter has established the physical, mathematical, and numerical foundations necessary for the simulation of the compact indirect solar dryer. The modeling is based on the fundamental equations of fluid mechanics and heat transfer, adapted to the specific features of solar drying. The finite volume method, implemented through ANSYS Fluent, provides a robust framework for solving and analyzing the performance of the system. These foundations will serve to interpret the simulation results in the following chapters.

Chapter III

Numerical Results, Analysis, and Interpretation

III.1. Introduction

This chapter presents the numerical results obtained from the simulation of the solar dryer system and provides a detailed analysis of the physical phenomena involved. The objective is to evaluate the thermal and aerodynamic behavior of the system under real operating conditions. Various key parameters, such as temperature distribution, air velocity, and heat transfer, are analyzed to understand the system's performance. To ensure the reliability and accuracy of the numerical model, a validation process is carried out by comparing the simulation results with experimental data.

III.2. Validation of Numerical Results

To validate the developed numerical model, à comparison was made between the simulated temperatures and the experimental data measured at key points of the solar dryer, particularly at the absorber, glass cover, and drying chamber. An inlet air velocity of 0.55 m/s was used. This velocity corresponds to one of the experimental conditions representative of the actual operation of the solar dryer.

The figure below shows the overlap of the experimental and numerical curves for the different zones of the dryer.

The graph above presents a comparison between the experimental and numerical temperatures as a function of time for three components of the indirect solar dryer: the absorber, the glazing, and the drying chamber. The absorber records the highest temperatures, reaching a maximum of approximately 70 °C experimentally and 69 °C numerically, which is explained by its position directly exposed to solar radiation. The glazing, on the other hand, shows a more moderate thermal evolution, with a maximum experimental temperature around 45 °C and a simulated value of about 41 °C. These temperatures are significantly lower than those of the absorber, confirming the passive role of the glazing, which transmits solar radiation into the system. Finally, the drying chamber exhibits the lowest temperatures, with a maximum of 39 °C experimentally and 37 °C in simulation. Overall, the numerical results closely follow the experimental trends, with moderate discrepancies that confirm the validity of the model. The temperature hierarchy (absorber > glazing > drying chamber) is well respected, indicating a good modeling of the system's thermal behavior.

In order to quantify the accuracy of the numerical model, a relative error analysis was carried out by comparing the simulated temperatures with the experimental values throughout the day.

The relative error was calculated using the following formula:

$$\textbf{Error}\ (\%) = \left| \frac{T_{Experimental} - T_{Numerical}}{T_{Experimental}} \right| \times 100 \qquad \text{III.1}$$

The table III.1 presents the average relative errors calculated for each component of the solar dryer. The evaluation of the average relative error between the experimental and numerical results confirms the quality of the modeling. The absorber shows the largest deviation, with an error of 6.4%. The glass cover displays a moderate error of 2.56%. An even more satisfactory result is observed in the drying chamber, with an error of only 0.755%. The overall average error is 3.23%, which remains well within the acceptable limits for the numerical simulation of a complex thermal system.

III.3. Effect of Air Velocity and thermal Behavior

➢ of 0.55 m/s:

Since the air velocity remains constant for all simulated time points, the analysis of the velocity effect was carried out based solely on the results obtained at 13h.

The figure shows the air velocity field in our solar dryer, obtained for an inlet velocity of 0.55 m/s. The velocity generally ranges between 0 and 2.07 m/s, with a maximum observed in the upper right section, just below the absorber, where the air movement is most intense. Inside the solar collector, velocities range between 0.55 and 1.4 m/s, indicating a rotational flow (presence of the one dominate vortex was observed.). In the drying chamber, there is a marked heterogeneity in velocity distribution. A central zone displays relatively low velocities, between 0.2 and 0.62 m/s. At the dryer outlet, the velocity ranges between 0.82 and 1.24 m/s. However, stagnant zones (or dead zones) appear in the upper and lower left corners, as well as near the outlet, where the velocity drops to as low as 0.2 m/s. These zones, characterized by poor air circulation, may negatively affect drying uniformity by slowing down the renewal of hot air around the products.

The study of thermal and dynamic behavior in our solar dryer was conducted at different times of the day (11h, 13h, 15h and 17h) with a constant inlet air velocity of 0.55 m/s. At 11h, the maximum temperature recorded in the drying chamber reaches 308 K (35°C), indicating the beginning of thermal rise. It gradually increases to a peak of 312 K (39°C) at 13h, corresponding to the maximum solar intensity. Subsequently, the temperature slightly decreases to 310 K (37°C) at 15h and then to 306 K (33°C) at 17h, following the decline in solar radiation at the end of the day. The observed heat in the chamber originates mainly from the lower part of the absorber.

- **of 0.65 m/s:**

The figure shows the air velocity field in our solar dryer, obtained for an inlet velocity of 0.65m/s. The velocity contour obtained for an inlet velocity of 0.65 m/s shows that the air velocity inside the dryer varies between 0 and 2.55 m/s. This variation indicates a non-uniform distribution of the airflow throughout the system. The highest velocities are generally observed near the outlet of the solar collector and in certain narrow areas of the airflow path, where the flow is accelerated. Conversely, low-velocity zones (close to 0 m/s) appear, particularly in the corners or recesses of the drying chamber, suggesting the presence of stagnant zones.

Figure III.5 illustrate the thermal and dynamic behavior in our solar dryer for an inlet air velocity of 0.65 m/s, at different times of the day (11h, 13h, 15h, and 17h).

At 11h, the maximum temperature reaches approximately 306 K (33°C), indicating the beginning of the thermal rise. This temperature increases to 310 K (37°C) around 13h, which corresponds to the peak of solar radiation and thus to the maximum heat transfer from the absorber to the drying chamber. Subsequently, a slight decrease is observed at 15h, with the temperature reaching 308 K (35°C), and it returns to 306 K (33°C) at 17h due to the gradual reduction in solar irradiation towards the end of the day.

- **of 0.45 m/s:**

Figure III.6 shows the air velocity field in our solar dryer, obtained for an inlet velocity of 0.45 m/s. The velocity contour shows that the air velocity throughout the entire dryer varies between 0 and 1.61 m/s. This variation reflects a non-uniform distribution of airflow across the different parts of the system. The highest velocities are generally observed in certain narrow areas of the circuit, particularly near the outlet of the solar collector, where the flow is accelerated. Conversely, low velocities, close to 0 m/s, appear in less active zones, such as corners or near the walls, indicating the presence of stagnant zones.

Figure III.7 illustrate the dynamic and thermal behavior in our solar dryer for an inlet air velocity of 0.45 m/s, at different times of the day (11h, 13h, 15h, and 17h).
At 11h, the maximum temperature reaches approximately 310 K (37°C), marking the beginning of the heating phase. The temperature then rises to a peak of 314 K (41°C) at 13h, corresponding to the maximum intensity of solar radiation. At 15h, a slight decrease is observed, with a temperature of 312 K (39°C), indicating the beginning of the decline in solar intensity. Finally, at 17h, the temperature remains relatively high, around 310 K (37°C).

- **Of 0.1 m/s:**

Figure III.8 shows the air velocity field in our solar dryer, obtained for an inlet velocity of 0.1 m/s. The velocity contour obtained for an inlet velocity of 0.1 m/s shows that the air velocity throughout the solar dryer ranges between 0 and 0.62 m/s. This low velocity range indicates a slow and relatively uniform flow in certain areas, although some heterogeneity in airflow distribution is still present. The highest velocities are mainly observed in narrow ducts or at the outlet of the collector, where the flow slightly accelerates. Conversely, very low velocities, close to 0 m/s, are observed in the center of the dryer, suggesting the presence of stagnant zones.

Figure III.9 show the thermal and dynamic behavior in our solar dryer for a very low inlet air velocity of 0.1 m/s. At 11h, 13h, and 15h, the maximum temperature reaches around 318 K (45°C), indicating significant thermal accumulation due to limited air renewal.

This low velocity increases the residence time of the hot air inside the dryer, thereby promoting a more pronounced temperature rise. At 17h, however, a noticeable temperature heterogeneity is observed, with values ranging from 310 K to 318 K (37°C-45°C). This uneven distribution is likely due to a decrease in solar radiation combined with weaker air circulation, which limits thermal mixing and favors the formation of cooler zones. This behavior highlights that very low airflow velocities can lead to poor temperature uniformity, which may negatively impact the overall drying efficiency.

III.4. Dynamic Behavior:

The analysis of the dynamic behavior of the air inside the dryer for inlet velocities of 0.55 m/s, 0.45 m/s, and 0.65 m/s reveals the formation of a large central vortex within the drying chamber. This main vortex indicates significant recirculation of hot air, showing that the airflow does not exit directly through the outlet but remains trapped in the volume, thus promoting prolonged thermal exchange. While this recirculation is beneficial for maintaining uniform temperatures, it may also slow down the renewal of humid air.

In addition to this primary vortex, several smaller vortices form in the upper and lower left corners of the dryer due to the angular geometry of the chamber, which creates zones of stagnation and low velocity. Another vortex is also observed near the outlet of the dryer.

For the very low velocity of 0.1 m/s, these vortex structures are much less developed, indicating a slower and les structured airflow in addition to this primary vortex, several smaller vortices form in the upper and lower left corners of the dryer due to the angular geometry of the chamber, which creates zones of stagnation and low velocity. Another vortex is also observed near the outlet of the dryer.

For the very low velocity of 0.1 m/s, these vortex structures are much less developed, indicating a slower and les structured airflow.

Figure III.10 showing the absorber temperatures for different inlet velocities (0.65, 0.55, 0.45, and 0.1 m/s) highlights that as the inlet velocity decreases, the absorber temperature increases. The highest temperature is observed for the lowest velocity (0.1 m/s). This can be explained by the fact that at low velocity, the air remains in contact with the absorber surface for a longer

period, allowing for more effective heat transfer. Conversely, when the inlet velocity increases, the contact time decreases.

The figure showing the temperatures in the drying chamber for different inlet velocities (0.65, 0.55, 0.45, and 0.1 m/s) indicates that the highest temperature is reached when the inlet velocity is the lowest, namely 0.1 m/s. It is observed that as the inlet velocity increases, the temperature in the drying chamber decreases. This phenomenon can be explained by the fact that at low velocity, the hot air moves more slowly, which increases its residence time in the chamber. Conversely, at higher velocities, the air passes through the chamber more quickly, reducing the heat exchange time and resulting in a lower overall temperature.

III.5. Effect of the Fan Position:

To study the effect of the fan position on the thermal and dynamic performance of the dryer, a new configuration was simulated. In this setup, the fan is placed at the outlet of the dryer, creating à negative pressure that draws air through the system. As a result, the boundary conditions were modified as follows:

- The inlet of the dryer is defined as a pressure inlet, allowing air to enter freely due to suction.
- The outlet is modeled with a specified velocity condition (Velocity Outlet), with a velocity of –0.55 m/s along the y-axis.

This configuration allows for the analysis of how the fan's position influences airflow circulation, temperature distribution, and overall drying efficiency at different times of the day.

III.5.1. Velocity behavior

Figure III.11 shows the airflow velocity field inside the dryer with a fan positioned at the outlet, imposing an exit velocity of -0.55 m/s along the y-axis (outflow). Air velocities now range between 0 and 1.55 m/s**,** indicating à more intense circulation. Higher velocities, between 0.62

and 1.24 m/s, are particularly observed in the solar collector area, which promotes better heat transfer between the air and the heated surfaces.

Additionally, air acceleration is noted near the outlet of the dryer, illustrating the effect of the fan by inducing more efficient extraction of hot air. However, in the center of the drying chamber, zones of low or nearly zero velocity persist, which could limit the uniform drying of the products placed in this region.

Compared to the previous configuration with a constant inlet velocity of 0.55 m/s, this new setup allows for a more varied and dynamic distribution of air velocity, with peaks well above 0.55 m/s. This enhances the renewal of hot air and the evacuation of moisture, thereby increasing the drying potential. However, the stagnation zones in the center indicate that, despite the addition of the fan, further optimization could be considered for example, by improving the internal distribution of the airflow.

III.5.2. Thermal and Dynamic Behavior:

The analysis of the thermal behavior in the dryer, with a fan placed at the outlet (simulation with pressure at the inlet and an outlet velocity of -0.55 m/s along the y-axis), shows à wellstructured temperature evolution throughout the day. The four temperature contours at 11h. 13h, 15h, and 17h. reveal a progressive thermal rise, reaching a maximum of 318 K (45°C) at 13h, the time of peak solar radiation. At 11h, the maximum temperature is 314 K (41°C), then it slightly decreases to 316 K (43°C) at 15h, and reaches 310 K (37°C) at 17h, following the typical solar radiation curve.

The introduction of a fan positioned at the outlet of the dryer, significantly alters the system's thermal and dynamic behavior. Unlike the previous cases (inlet velocities of 0.55, 0.65, and 0.45 m/s), where a vortex persisted near the dryer outlet, this new configuration eliminates the local swirl. The suction effect induced by the fan promotes à more direct and linear airflow toward the exit, improving the evacuation of hot and humid air.

As a result, the airflow becomes more homogeneous, with à notable reduction in stagnation zones and a more efficient circulation throughout the drying chamber.

This change also leads to a more stable thermal distribution, showing that the presence of the fan enhances the dryer's overall performance by facilitating air renewal and reducing unwanted recirculations. The addition of the fan not only improves airflow dynamics but also stabilizes heat distribution, which is favorable for more uniform drying.

III.6. Collector Efficiency

The instantaneous thermal efficiency of the solar collector is calculated using the following relation:

$$\eta_{co} = \frac{\dot{m}.C_p.(T_{out} - T_{in})}{I.A_c} \qquad \text{III.2}$$

- η_{co} : Thermal efficiency of the solar collector.
- $\dot{m}$:Mass flow rate of air [kg/s].
- C_p : Specific heat capacity of air [J/Kg·K].
- T_{out} : Air temperature at the outlet of the collector [°C].
- T_{in} : Air temperature at the inlet of the collector [°C].
- I : Incident solar radiation [W/m²].
- A_c : Collector surface [m²].

Figure III.13 shows the variation of the solar collector efficiency over time for a velocity inlet of 0.55m/s. It can be observed that the efficiency curve of the solar collector exhibits a nonmonotonic evolution throughout the day, with several phases of increase and decrease. This fluctuation can be explained by multiple factors influencing the instantaneous efficiency of the collector.

In the morning, the efficiency tends to gradually increase as solar radiation intensifies and the collector temperature rises. However, as the fluid temperature increases, part of the received energy is lost as heat through convection and radiation, which can cause a temporary drop in efficiency.

Around midday, variations in the incident solar radiation, as well as the rise in ambient temperature, may disrupt thermal performance. These fluctuations thus reflect the combined influence of solar radiation, thermal losses, and ambient conditions on the actual operation of the collector.

The maximum efficiency recorded during the day reaches 0.87, while the average efficiency is approximately 0.45, indicating a relatively effective thermal conversion over the entire operating period.

III.7. Drying Chamber Efficiency

The instantaneous thermal efficiency of the drying chamber is calculated using the following relation:

$$\eta_{ch} = \frac{\dot{m}.Cp.(Tout\ ch - Tin\ ch)}{\dot{m}.Cp.(Tout\ ch - Tin\ cap)} \quad \text{III.3}$$

Where:

- η_{ch}= thermal efficiency of the drying chamber.
- $\dot{m}$= mass flow rate of air (Kg/s).
- C_p = specific heat capacity of air (J/Kg·K).
- $T_{out\ ch}$ = air temperature at the outlet of the drying chamber (°C).
- $T_{in\ ch}$ = air temperature at the inlet of the drying chamber (°C).
- $T_{in\ cap}$ = air temperature at the inlet of the solar collector (°C).

The evolution of the thermal efficiency of the drying chamber throughout the day shows a clear dependence on solar conditions. From 10:00 to 13:00, the efficiency generally increases, reaching a maximum value around 13:00, which corresponds to peak solar radiation. This indicates that the drying chamber operates optimally during midday hours. However, after 13:00, a sharp decrease in efficiency is observed. This drop may be attributed to reduced solar intensity, increased humidity inside the chamber, or thermal losses. Between 14:00 and 16:00, the efficiency remains relatively low but shows a slight upward trend, suggesting a partial recovery as solar conditions stabilize.

The maximum recorded thermal efficiency is 0.99, while the average efficiency throughout the day is 0.69**.**

III.8. Conclusion

This chapter presents the validation of the numerical model by comparison with experimental results. The simulations provided valuable data on temperature distribution and airflow velocity within the various components of the dryer, contributing to a deeper understanding of the

system’s thermal and dynamic behavior. The system achieved an average thermal efficiency of 45 % in the solar collector and 69 % in the drying chamber.

General Conclusion

General conclusion

This study examines the dynamic and thermal behavior of a compact indirect solar dryer, based on experimental data. The simulation is carried out using Ansys Fluent 19 software.

The results obtained in this study highlight the reliability and efficiency of numerical modeling applied to an indirect solar dryer. Initially, the comparison between numerical and experimental results for an inlet velocity of 0.55 m/s showed good agreement, with an overall error of 3.23%.

An increase in the inlet velocity leads to a rise in air circulation speed within the drying chamber. For inlet velocities of 0.1 m/s, 0.45 m/s, 0.55 m/s, and 0.65 m/s, the maximum recorded speeds are 0.62 m/s, 1.61 m/s, 2.07 m/s, and 2.55 m/s respectively.
The temperature inside the dryer increases until reaching a peak around 13h., then decreases. Lower inlet velocities allow for higher temperatures due to the longer residence time of hot air. At 13h., the maximum temperatures recorded were: 45 °C, 41 °C, 39 °C, and 37 °C for 0.1 m/s, 0.45 m/s, 0.55 m/s, and 0.65 m/s respectively.

The simulations revealed the presence of air vortices inside the dryer, including one near the outlet which limits the renewal of hot air. By placing the fan at the outlet with a velocity of v = -0.55 m/s, this vortex disappears, making the flow more laminar. This configuration optimizes drying, reaching 1.55 m/s and 45 °C at 13:00.

Finally, the dryer achieved a maximum thermal efficiency of up to 87% and an average thermal efficiency of 45%. The maximum recorded thermal efficiency in the drying chamber is 99%, while the average efficiency throughout the day is 69 % .

The thermal efficiency of the solar collector and the drying chamber confirms the good overall performance of the system

In conclusion, this study demonstrates that numerical simulation is an effective tool for analyzing and optimizing the operation of an indirect solar dryer. It not only validates the initial design but also enables consideration of future improvements by adjusting parameters such as speed, temperature, and internal configuration to maximize drying performance.

General conclusion

In a future perspective, we plan to study mass conservation in order to analyze the drying process of different products using our solar dryer.

References

[1] Md Zillur Rahman, Md Hasanuzzaman. Solar drying system. Technologies for solar thermal energy: theory, design, and optimization. P.237-266,2022.

[2] KHALDI, Souheyla, Etude numérique du comportement thermique d'un séchoir solaire utilisant un lit thermique pour le stockage d'énergie. Thèse de doctorat. Université Bourgogne Franche-Comté ; Université Abou Bekr Belkaid (Tlemcen, Algérie) .2018

[3] BELESSIOTIS, V. et DELYANNIS, E. Solar drying. Solar energy, vol. 85, N°8, p. 16651691.2011.

[4] AZZOUZ Ismahan, TAOURIT Mohammed El Amine, Modélisation et amélioration des performances d'un séchoir solaire indirect à convection naturelle, Mémoire de Master, Université Abou Bekr Belkaid (Tlemcen, Algérie).2021.

[5] Bahadj, Ahmed. Etude Expérimentale De Séchage Solaire De La Pomme De Terre, Mémoire de Master, Université Kasdi Merbah - Ouergla.2014

[6] Boutalbi Adel, Mokrani elmahdi. Etude expérimentale du séchage des petits pois, Mémoire de Master, Université de Biskra.2022.

[7] Hany S. EL-Mesery, Ahmed I. EL-Seesy, Zicheng Hu , Yang Li , Recent developments in solar drying technology of food and agricultural products. Renewable and Sustainable Energy Reviews. Volume 157, April 2022.

[8] A.G.M.B. Mustayen, S. Mekhilef, R. Saidur. Performance study of different solar dryers: A review. Renewable and Sustainable Energy Reviews, vol. 34, p. 463-470, June 2014.

[9] OULAD BELKHIER, Oussama et MOULAY BRAHIM, Abdelbasset. Conception, Réalisation et investigation expérimentale d'un procédé de séchage solaire avec système de stockage d'énergie thermique, Thèse de doctorat, Université Ghardaia, 2022.

[10] SHEKATA, Gadisa Desa, TIBBA, Getachew Shunki, et BAHETA, Aklilu Tesfamichael. Recent advancements in indirect solar dryer performance and the associated thermal energy storage. Results in Engineering, Volume 157, 2024.

References

[11] CHAUDHARI, Ashish D. et SALVE, Sanjay P. A. review of solar dryer technologies. International Journal of Research in Advent Technology, vol. 2, no 2, p. 218-232, Reference ,2014.

[12] SHARMA, Atul, CHEN, C. R., et LAN, Nguyen Vu. Solar-energy drying systems: A review. Renewable and sustainable energy reviews, vol. 13, no 6-7, p. 1185-1210, 2009.

[13] BALASUADHAKAR, A., FISSEHA, Teklebirhan, ATENAFU, Amessalu, et Bariso Bino. A review on passive solar dryers for agricultural products. International Journal for Innovative Research in Science & Technology, vol. 3, no 01/13, p. 64-70, 2016.

[14] KHERROUR, S., BEKKOUCHE, S. M. A., et SERIR, L. Comportement thermique d'un séchoir solaire direct type serre dans la région de Ghardaïa. 2ème Séminaire Maghrébin sur les Sciences et les Technologies de Séchage, p. 20-22, 2008.

[15] CHAVAN, Anand, VITANKAR, Vivek, MUJUMDAR, Arun, et Bhaskar Thorat. Natural convection and direct type (NCDT) solar dryers: à review. Drying Technology, vol. 39, no 13, p. 1969-1990.2021.

[16] KANOUNE, Brahim et TRITIBA, Abdeslam. Etude et amélioration de l'efficacité énergétique d'un séchoir solaire direct à convection naturelle. UNIVERSITÉ KASDI MERBAH OUARGLA, Thèse de doctorat.2016

[17] ZENGUI, Bachir et MANSOURI, Saïd. Etude de l'effet de l'intégration d'une couche MCP sur les performances d'un séchoir solaire direct, Université Kasdi Merbah Ouargla, Mémoire de Master ,2017.

[18] DINA, Sari Farah, AMBARITA, Himsar, NAPITUPULU, Farel H., etHideki Kawai. Study on effectiveness of continuous solar dryer integrated with desiccant thermal storage for drying cocoa beans. Case Studies in Thermal Engineering, vol. 5, p. 32-40, 2015.

[19] SHAMEKHI-AMIRI, Shahrbanou, GORJI, Tahereh B., GORJI-BANDPY, Mofid, et Mohammad Jahanshahi. Drying behaviour of lemon balm leaves in an indirect double-pass packed bed forced convection solar dryer system. Case studies in thermal engineering, vol. 12, p. 677-686, September2018.

[20] AMEUR Khadidja BENOSMANE Imane, Réalisation expérimentale d'un séchoir solaire indirect, Mémoire de Master, Université Abou Bekr belkaid Tlemcen, 2023

References

[21] LOUAZENE, Abderrahmane et BOUHNIK, Abdallah. Etude Numérique d'une Cheminée Solaire à MCP Intégré Destinée à la Ventilation d'un Séchoir Solaire. Thèse de doctorat. Université Kasdi Merbah Ouargla, 2017.

[22] UGWUOKE, Ikechukwu Celestine, IKECHUKWU, Ibukun Blessing, et IFIANYI, Ogbe Eric. Design and development of a mixed-mode domestic solar dryer. International Journal of Engineering and Manufacturing, p.55-65, 2019.

الملخص

تتناول هذه الدراسة تحليل السلوك الحراري الديناميكي لمجفف شمسي غير مباشر مدمج. وتهدف إلى وصف ظواهر انتقال الحرارة داخل النظام، مع التركيز بشكل خاص على آليات التوصيل الحراري المضطر والطبيعي، بالإضافة إلى توزيع درجات الحرارة داخل مكونات المجفف المختلفة. يعتمد الجهاز المدروس على مجمّع شمسي حراري متصل بغرفة تجفيف معزولة، مما يسمح بانتقال الحرارة من خلال تدفق هواء ساخن، دون تعريض المنتج مباشرةً للإشعاع الشمسي. تتم دراسة المحاكاة العددية المدعومة ببيانات تجريبية، من أجل تقييم الكفاءة الطاقوية للنظام وتحسين معاملات التشغيل
.

الكلمات المفتاحية: مجفف شمسي غير مباشر مدمج، السلوك الحراري الديناميكي، محاكاة عددية

Résumé

Cette étude porte sur l'analyse du comportement thermo-dynamique d'un séchoir solaire indirect compact.
L'objectif est de caractériser les phénomènes de transfert de chaleur intervenant dans le système, en mettant particulièrement l'accent sur les mécanismes de convection forcée et naturelle, ainsi que sur la distribution des températures au sein des différentes composants du séchoir. Le dispositif étudié repose sur un capteur solaire thermique couplé à une chambre de séchage isolée, permettant un transfert de chaleur par l'intermédiaire d'un flux d'air chauffé, sans exposition directe du produit au rayonnement solaire. Une modélisation numérique, éventuellement couplée à des données expérimentales, est envisagée afin d'évaluer l'efficacité énergétique du système et d'optimiser les paramètres de fonctionnement.

Mots clés : séchoir solaire indirect compact, comportement thermique dynamique, convection forcée et naturelle, Modélisation numérique

Abstract

This study focuses on the analysis of the thermo-dynamic behavior of a compact indirect solar dryer. The objective is to characterize the heat transfer phenomena occurring within the system, with particular emphasis on the mechanisms of forced and natural convection, as well as the temperature distribution within the different components of the dryer. The studied device is based on a thermal solar collector coupled with an insulated drying chamber, allowing heat transfer through a flow of heated air without direct exposure of the product to solar radiation. A numerical modeling approach, possibly supported by experimental data, is considered in order to evaluate the energy efficiency of the system and optimize its operating parameters.

Keywords: compact indirect solar dryer, dynamic thermal behavior, forced and natural convection, numerical modeling.